

5.0
AFWAL-TR-80-3027

LEVEL

(2)

ADA 087709

DEVELOPMENT OF A NOZZLE TO IMPROVE THE TURNING OF SUPERSONIC COANDA JETS

Paul M. Bevilaqua

*Rockwell International
North American Aircraft Division
Columbus, Ohio 43216*

John D. Lee

*Ohio State University
Dept. of Aeronautical and Astronautical Engineering
Columbus, Ohio 43210*

APRIL 1980

TECHNICAL REPORT AFWAL-TR-80-3027
Final Report for Period 15 June 1979-15 March 1980

Approved for public release; distribution unlimited.

DC FILE COPY

FLIGHT DYNAMICS LABORATORY
AIR FORCE WRIGHT AERONAUTICAL LABORATORIES
AIR FORCE SYSTEMS COMMAND
WRIGHT-PATTERSON AIR FORCE BASE, OHIO 45433

DTIC
ELECTE
S AUG 8 1980 D

A


1.

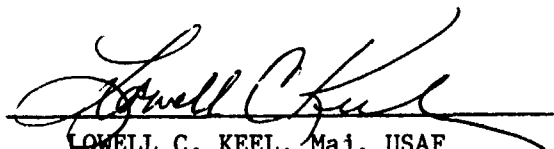
NOTICE

When Government drawings, specifications, or other data are used for any purpose other than in connection with a definitely related Government procurement operation, the United States Government thereby incurs no responsibility nor any obligation whatsoever; and the fact that the government may have formulated, furnished, or in any way supplied the said drawings, specifications, or other data, is not to be regarded by implication or otherwise as in any manner licensing the holder or any other person or corporation, or conveying any rights or permission to manufacture use, or sell any patented invention that may in any way be related thereto.

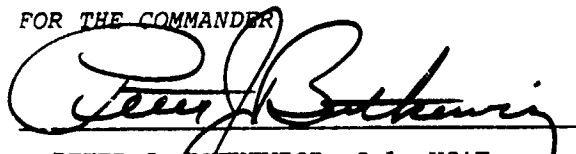
This report has been reviewed by the Office of Public Affairs (ASD/PA) and is releasable to the National Technical Information Service (NTIS). At NTIS, it will be available to the general public, including foreign nations.

This technical report has been reviewed and is approved for publication.


JAMES A. LAUGHREY
Project Engineer


LOWELL C. KEEL, Maj, USAF
Chief, Aerodynamics & Airframe Branch
Aeromechanics Division

FOR THE COMMANDER


PETER J. BUTKEWICZ, Col, USAF
Chief, Aeromechanics Division

"If your address has changed, if you wish to be removed from our mailing list, or if the addressee is no longer employed by your organization please notify AFWAL/FIMM W-PAFB, OH 45433 to help us maintain a current mailing list".

Copies of this report should not be returned unless return is required by security considerations, contractual obligations, or notice on a specific document.

SECURITY CLASSIFICATION OF THIS PAGE (When Data Entered)

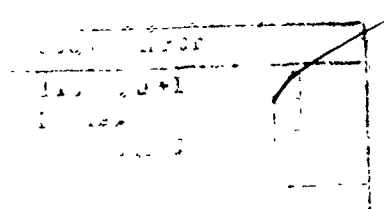
19 REPORT DOCUMENTATION PAGE		READ INSTRUCTIONS BEFORE COMPLETING FORM	
1 REPORT NUMBER AFWAL-TR-80-3027	2 GOVT ACCESSION NO. AD-A087709	3 RECIPIENT'S CATALOG NUMBER	
4 TITLE (and Subtitle) Development of a Nozzle to Improve the Turning of Supersonic Coanda Jets		5 TYPE OF REPORT & PERIOD COVERED Final Report 15 June 1979 - 15 March 1980	
7 AUTHOR(s) P. M. Bevilaqua, Rockwell International Corp. J. D. Lee, Ohio State University		6 PERFORMING ORG REPORT NUMBER NR80H-18	
9 PERFORMING ORGANIZATION NAME AND ADDRESS Rockwell International Corp. North American Aircraft Division Columbus, Ohio 43216		8 CONTRACT OR GRANT NUMBER(s) F33615-79-C-3026	
11 CONTROLLING OFFICE NAME AND ADDRESS USAF, Wright Aeronautical Laboratories Flight Dynamics Laboratory (AFWAL/FIMM) Wright-Patterson AFB, Ohio 45433		10 PROGRAM ELEMENT, PROJECT, TASK AREA & WORK UNIT NUMBERS 24041044	
14 MONITORING AGENCY NAME & ADDRESS (if different from Controlling Office) 10) Paul M. Bevilaqua John D. Lee		12 REPORT DATE April 1980	
		13 NUMBER OF PAGES 49	
		15 SECURITY CLASS (of this report) Unclassified	
		15a DECLASSIFICATION DOWNGRADING SCHEDULE	
16 DISTRIBUTION STATEMENT (of this Report) Approved for Public Release, Distribution Unlimited			
17 DISTRIBUTION STATEMENT (of the abstract entered in Block 20, if different from Report)			
18 SUPPLEMENTARY NOTES			
19 KEY WORDS (Continue on reverse side if necessary and identify by block number) Coanda Effect Powered Lift Thrust Vectoring STOL/VSTOL Nozzle Flows Turbulence			
20 ABSTRACT (Continue on reverse side if necessary and identify by block number) The hypothesis that shaping the jet velocity profile improved the thrust vectoring of supersonic Coanda jets was experimentally tested. A new nozzle design procedure, based on the method of characteristics, was developed to design a nozzle which delivers an arbitrary exit velocity profile. Such a nozzle was designed for a pressure ratio of 2.5, to provide a jet matched to a circular Coanda surface with radius equal to five jet thicknesses. The thrust vectoring of this nozzle was then compared to that of a convergent			

divergent nozzle over a range of pressure ratios from 1.5 to 3.5. It is concluded that supersonic nozzles provide greatly improved turning of Coanda jets, and that shaping the velocity profile further improves the thrust vectoring.

FOREWORD

This report describes work performed by the North American Aircraft Division of Rockwell International during the period from 15 June 1979 to 15 March 1980. This work was supported by the U. S. Air Force Wright-Aeronautical Laboratories under Contract F33615-79-C-3026. The technical monitor was Mr. J. A. Laughrey of the Flight Dynamics Laboratory.

We would like to acknowledge the contributions of Mr. Paul Cole and Mr. Robert Cooke, who helped to plan and run the tests, and Mr. Thomas Barnes, who developed the data acquisition routines which were employed.



A

TABLE OF CONTENTS

SECTION		PAGE
I	INTRODUCTION	1
II	COANDA JET ATTACHMENT AND SEPARATION	4
III	NOZZLE DESIGN PROCEDURE.	8
	Method of Analysis.	8
	One-Step Design Approach.	13
	Design of the Nozzles	18
IV	EXPERIMENTAL APPARATUS	21
	Description of the Model.	21
	Instrumentation	23
V	RESULTS AND DISCUSSION	24
	Balance Measurements.	24
	Surface Pressure Measurements	27
	Total Pressure Profiles	31
	Schlieren Photographs	34
VI	CONCLUSIONS.	39
	APPENDICES	40
	REFERENCES	48

PRECEDING PAGE BLANK-NOT FILMED

LIST OF FIGURES

FIGURE		PAGE
1	Use of the Coanda Effect for Thrust Vectoring. . .	1
2	Balance of Forces in a Coanda Jet.	5
3	Boundary Layer Separation due to Reflected Expansion Waves.	7
4	Conditions at c Are Determined by Characteristics for a and b.	9
5	Schematic of Coanda Jet Characteristics.	12
6	Course Net for the Nozzle Design Procedure	14
7	Fine Net Operator for the Nozzle Design Procedure.	15
8	Exit Velocity Profiles for which the Nozzles Were Designed	19
9	Contours of the Conventional and Vortex Nozzles. .	20
10	Vortex Turning Nozzle on 6-Component Balance . . .	21
11	Location of the Pressure Taps on the Nozzle and Coanda Surface	22
12	Variation of Jet Turning Angle with Nozzle Pres- sure Ratio	24
13	Variation of Jet Turning Efficiency with Nozzle Pressure Ratio	26
14	Variation of Jet Mass Flow with Nozzle Pressure Ratio.	27
15	Static Pressure Difference ($P-P_{\infty}$) over the Con- vergent-Divergent Nozzle	8
16	Static Pressure Difference ($P-P_{\infty}$) over the Vortex Nozzle	29
17	Comparison of Predicted and Measured Pressures in the Conventional Nozzle.	30

LIST OF FIGURES (Cont'd)

FIGURE		PAGE
18	Comparison of Predicted and Measured Pressures in the Vortex Nozzle.	31
19	Predicted and Measured Total Pressure Profiles at the Exit of the Vortex Nozzle.	32
20	Development of the Total Pressure Profiles from the Conventional Nozzle.	33
21	Development of the Total Pressure Profiles from the Vortex Nozzle.	33
22	Schlieren Photographs of the Coanda Jets from the Convergent-Divergent Nozzle.	35
23	Schlieren Photographs of the Coanda Jets from the Vortex Profile Nozzle.	36
24	Schlieren Photographs of the Coanda Jets from the Convergent Nozzle.	37

NOMENCLATURE

C_f	compressible flow friction coefficient
C_{fi}	incompressible flow friction coefficient
F_x	horizontal component of the jet thrust
F_y	vertical component of the jet thrust
H	velocity profile shape factor
L, R	left and right characteristic wave constants
M	Mach number
P	fluid pressure
P_∞	ambient pressure
P_o	stagnation pressure
R	radius of streamline curvature
R	gas constant
Re	Reynolds number of the jet flow
Re_θ	Reynolds number of the boundary layer
S	local slope of the characteristics
T	jet momentum
T_o	stagnation temperature
V	jet velocity
x, y	Cartesian coordinate directions
K	vortex profile constant
\dot{m}	mass flow
r, θ	radial coordinate directions
t	initial jet thickness
α	Mach angle
δ	jet thickness
γ	ratio of specific heats
μ	fluid viscosity
ν	Prandtl-Myer function
ρ	fluid density
ϕ_{sep}	Coanda jet separation angle
ϕ_{def}	Coanda jet deflection angle
ω	angular direction of flow

SECTION I

INTRODUCTION

In order to meet the anticipated requirement for aircraft which can operate from damaged or unprepared airfields, the U. S. Air Force is studying various means of developing the additional low speed lift required by short takeoff and landing (STOL) aircraft. A particularly simple and, therefore, attractive approach is to utilize the Coanda effect¹ to deflect the thrust of a turbojet engine, as shown in Figure 1. The Coanda effect is the tendency for a fluid jet to attach itself to an adjacent surface and follow its contour. The application of this phenomenon to several thrust vectoring and lift augmentation concepts is currently being investigated. For example, both the YC-14² and QSRA³ STOL transport aircraft employ the Coanda effect for thrust deflection. Coanda jets are also incorporated in the inlet of the ejectors being developed for the XFV-12A aircraft⁴ and at the trailing edge of the

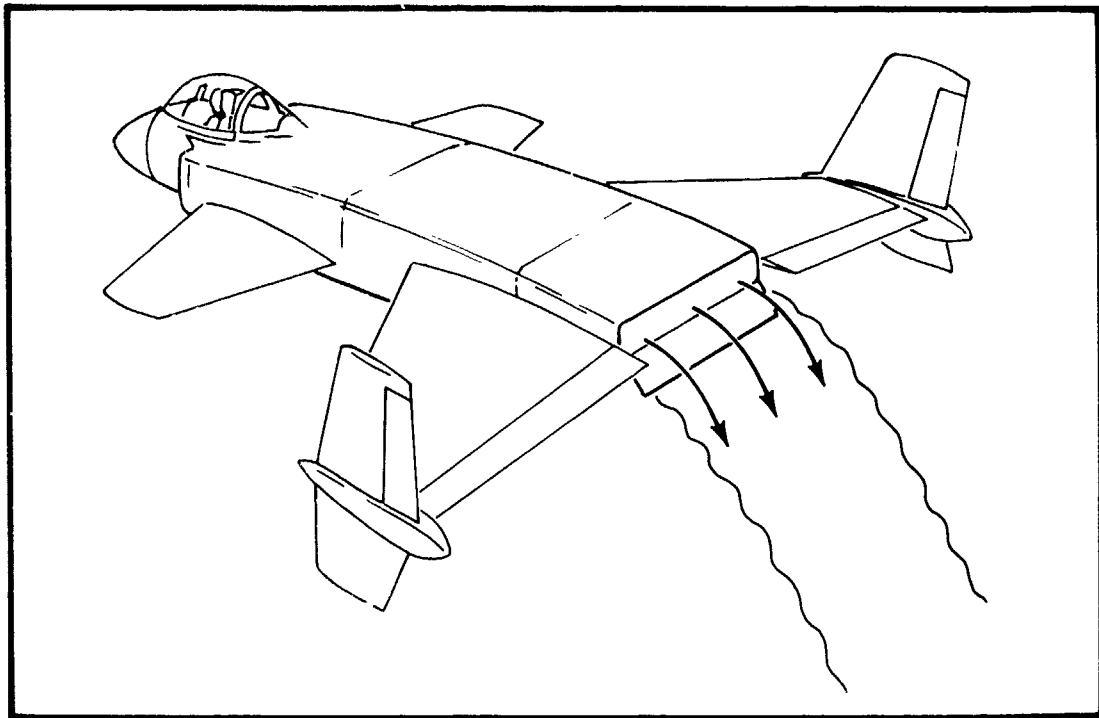


Figure 1. Use of the Coanda Effect for Thrust Vectoring

circulation control wing being tested on a modified A6 aircraft.⁵ Additional applications of the Coanda effect are envisioned for the vectored-engine-over-wing STOL fighter⁶ and the HiMAT transonic maneuvering fighter.⁷

The STOL performance of all these aircraft depends on deflecting the engine exhaust jet through a relatively large angle. If the radius of the Coanda surface is large compared to the initial jet thickness, such angles are easy to obtain; the jet remains attached to the surface through deflection angles of more than 180° . However, if the radius of curvature is small, the jet resists deflection and may not attach to the surface at all. Because size and weight limitations tend to keep the radius of aircraft deflection surfaces small, large deflection angles have been difficult to obtain. Deflections of less than 60° are typical of aircraft systems being developed.

The purpose of this report is to describe a nozzle designed to improve the turning of supersonic Coanda jets, by reducing the resistance of the jet to deflection. A Coanda jet is pulled around the surface by the low pressure which develops as entrainment pumps fluid from the region between the jet and the surface. The jet is then held to the wall by a radial pressure gradient, with low pressure at the surface, which balances the inertial resistance of the jet. A jet having a uniform "top hat" velocity profile resists deflection because the radial pressure gradient is zero at the nozzle exit. Even if the jet is deflected, the turning shocks which then develop may cause it to separate again within a short distance.

However, a nozzle can be designed to produce a skewed velocity distribution. If the high-velocity, low pressure side is on the surface, the tendency for the jet to deflect in that direction will aid it in flowing around the Coanda surface. By suitable shaping of the velocity profile, the jet deflection can theoretically be matched to the curvature of the Coanda surface. For example, the streamlines of an irrotational vortex flow are circular, and the velocity varies inversely with distance from

the center of rotation. A jet having such a velocity distribution can be matched to the radius of a circular Coanda surface, and should flow around that surface without turning losses. This concept has already been used to develop an "aerodynamic window" for gas dynamic lasers;⁸ in that application, the jet curvature supports the low pressure in the laser cavity.

The objective of this research is to evaluate the hypothesis that shaping the jet velocity profile improves the thrust vectoring of supersonic Coanda jets. This was accomplished by designing a convergent/divergent nozzle which produces a skewed velocity profile, and comparing its deflection angle and thrust to that of a conventional convergent/divergent nozzle. A new nozzle design procedure, based on the method of characteristics, was devised to define the nozzle contour. In the next section of this report, the factors which affect the turning of Coanda jets are analyzed in more detail. The design procedure and the contours of the nozzles which were tested are discussed in the following section. The test apparatus and instrumentation are then described. In the last section, the test results are presented and evaluated. It is concluded that convergent/divergent nozzles provide greatly improved turning compared to the simple convergent nozzles now being used, and that shaping the velocity profile further improves the thrust vectoring.

SECTION II

COANDA JET ATTACHMENT AND SEPARATION

It is not generally recognized that there are actually two problems of Coanda jet deflection over small radius curves (generally, with a radius of less than 10 jet thicknesses): that of initially attaching the jet, and that of delaying the eventual separation of the attached jet. The inertia of the jet stream resists the initial attachment of the jet. If the inertial force, $\rho v^2/R$, which increases as the radius of the turn decreases, becomes larger than the radial pressure gradient, $\partial P/\partial r$, which draws the jet toward the surface, the jet will not attach. Attachment limits have not been established, but the minimum radius of attachment decreases with increasing jet Mach number.⁹ The use of external deflector vanes, which act to turn the jet toward the surface, has been suggested to aid attachment of the jet in this case.¹⁰ Another approach has been to use surface mounted director vanes, which spread the jet out to reduce its thickness, and thus increase the effective turning radius.²

In the absence of external disturbances, a jet which has attached to a flat plate will remain attached. However, a jet which has attached to a curved plate will eventually separate, due to the action of viscosity. Viscosity causes the development of a boundary layer at the inner edge of the jet, and a mixing layer at the outer edge, where the surrounding fluid is entrained. It is the entrainment of the surrounding fluid which actually causes the boundary layer to separate. This occurs in the following way: as the jet flows around the curved surface, the inertia force is balanced by the radial pressure gradient; that is,

$$\frac{\partial P}{\partial r} = \frac{\rho v^2}{R} \quad 2.1$$

as shown schematically in Figure 2. Dimensionally, this equation may be interpreted as

$$\frac{\Delta P}{\delta} \sim \frac{\rho v^2}{R} \quad 2.2$$

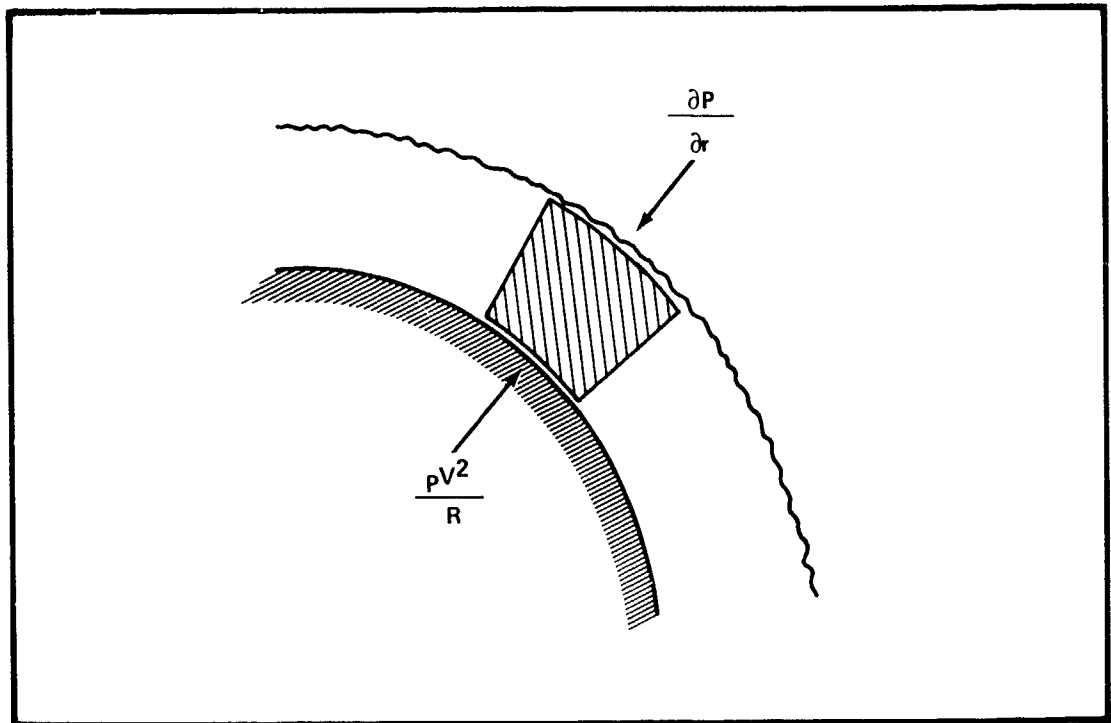


Figure 2. Balance of Forces in a Coanda Jet

in which δ is the thickness of the jet. Thus, to first order, the pressure on the Coanda surface is given by

$$P(\phi) = P_{\infty} - T(\phi)/R(\phi) \quad 2.3$$

in which T is the local momentum of the jet. As the jet flows around the surface, its thrust is reduced by wall friction and the average radius of curvature is increased by mixing with the surroundings. Both these effects cause the surface pressure to rise. The jet boundary layer eventually separates in the resulting adverse pressure gradient. Of course, the boundary layer may separate sooner, if a more severe gradient is imposed on it, as by an impinging shock wave.

There are no theories for predicting the point of separation. But, if it is assumed that the separation angle depends on the initial thrust of the jet, the radius of the Coanda surface, and the properties of the fluid, dimensional analysis gives

$$\phi_{\text{sep}} = f(R/t, Re, M) \quad 2.4$$

Re and M are the jet Reynolds number and Mach number, respectively. The form of this function can be determined from experimental data. Although not enough data has been obtained to do so, the value of this function has been determined in some limiting cases: for incompressible flow ($M = 0$), Newman¹¹ found that the separation angle increases with R/t and Re to a maximum value of about 245° . At $R/t = 5$, the turning angle is about 170° . In the transonic regime, Davenport and Hunt² did not obtain more than 100° of turning, and achieved only about 60° at $R/t = 5$. There is very little data for supersonic Coanda jets, but Bradbury and Wood⁹ found that the separation angle decreases as the Mach number is increased. All these data were obtained with convergent nozzles.

Two methods of boundary layer control have previously been proposed to prevent the separation of attached Coanda jets. Both Coanda¹ and von Glahn¹² studied the effectiveness of multiple flat plate turning surfaces, whose corners were intended to trip the boundary layer and thus increase its energy. Not enough data was obtained to show a clear advantage. Bradbury and Wood⁹ also examined the effect of auxiliary blowing slots on the turning surface. These were found to be effective for subsonic jets, but had no influence on supersonic jets. Davenport and Hunt² compared the jet turning performance of a series of two piece flaps, which consisted of a circular arc followed by a straight section. The jet was found to be turned further by a flap with a small initial radius followed by a straight section than by a flap the same length but with a larger radius.

Matching the jet velocity profile to the curvature of the Coanda surface, which is the object of this study, may be expected to influence both the attachment and separation of the Coanda jet. In a subsonic jet, the flow along the inner wall of the nozzle accelerates as it approaches the Coanda surface, so that the velocity profile is skewed at the nozzle exit. The resulting radial pressure gradient enables the jet to turn onto the Coanda surface. This adjustment is made naturally, since the

influence of the curvature is transmitted upstream in a subsonic jet. Because a supersonic jet cannot make this adjustment, it resists turning. Thus, designing the nozzle to skew the velocity profile is intended to overcome the resistance to turning in this case.

If the entrainment of the jet is strong enough, the resulting low pressure will force the jet to deflect onto the Coanda surface, in spite of its resistance. In this case, a system of expansion waves will form on the Coanda surface, as sketched in Figure 3. These waves will be reflected from the outer boundary of the jet as a compression (shock) wave, and impinge on the boundary layer. If the impinging shock is strong enough, the jet will separate from the surface at this point. Skewing the velocity profile to match the jet curvature to the surface curvature will prevent the formation of this wave system. Thus, the jet should remain attached to the surface until viscous effects cause eventual separation.

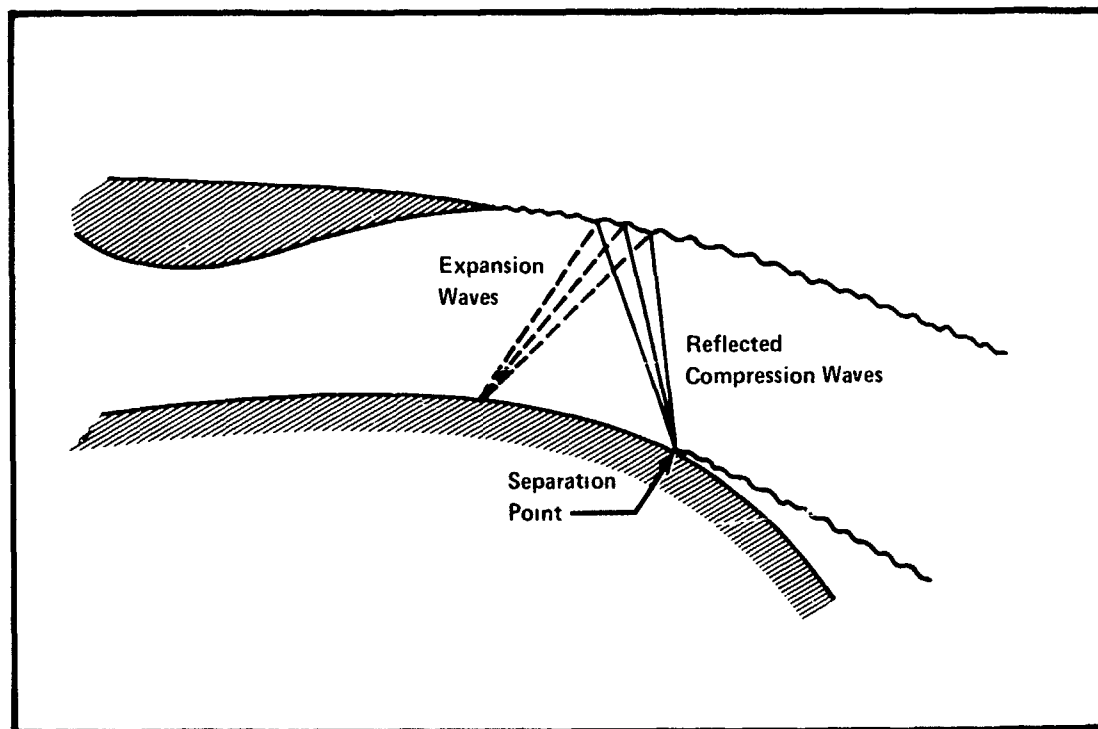


Figure 3. Boundary Layer Separation Due to Reflected Compression Waves

SECTION III

NOZZLE DESIGN PROCEDURE

Method of Analysis

Although a method of designing nozzles which deliver a free vortex ($V = k/R$) velocity profile was developed by Guile⁸ for his work on aerodynamic windows, it was felt a more flexible procedure was needed for Coanda jet applications. Guile's method involves first expanding the flow to some uniform Mach number and then expanding the flow further in order to skew the velocity profile. Such a "two stage" design procedure results in a nozzle which is too long for most aircraft systems. Further, this approach places some restrictions on the shape of the exit velocity profile, which then limits the shape of the Coanda surface.

Therefore, a method of designing a "single stage" nozzle which delivers an arbitrary exit velocity profile was developed for this study. In order to determine what reduction in nozzle length this method provided, it was then used to design a free vortex nozzle. The nozzle was designed for a pressure ratio of 2.5 and Coanda turning radius of five jet thicknesses, which were chosen as typical of thrust vectoring systems on STOL aircraft. The program was also used to design a conventional convergent-divergent nozzle for the same mass flow. The performance of these nozzles was then compared by building and testing both of them.

An inverse method of characteristics procedure was developed to design the nozzles. The method of characteristics is a procedure for the analysis of continuous supersonic flow fields. By combining the equations of mass, momentum, and energy conservations, a transformation of coordinates into a non-orthogonal system oriented to the local Mach angle yields a peculiar set of equations in the Mach directions.¹³ These equations are $\theta \pm \nu =$ constants at any given point in the field, where θ is the flow direction referenced to some arbitrary fixed reference and ν is the Prandtl-Meyer function,

$$\nu = \left[\frac{\gamma+1}{\gamma-1} \right]^{1/2} \tan^{-1} \left[\left[(M^2 - 1) \frac{\gamma-1}{\gamma+1} \right]^{1/2} - \tan^{-1} (M^2 - 1)^{1/2} \right] \quad 3.1$$

and the constants are fixed in the two Mach directions or characteristics. This result may be used to construct solutions to supersonic flow fields by an application of the following principles and equations, as illustrated in Figure 4.

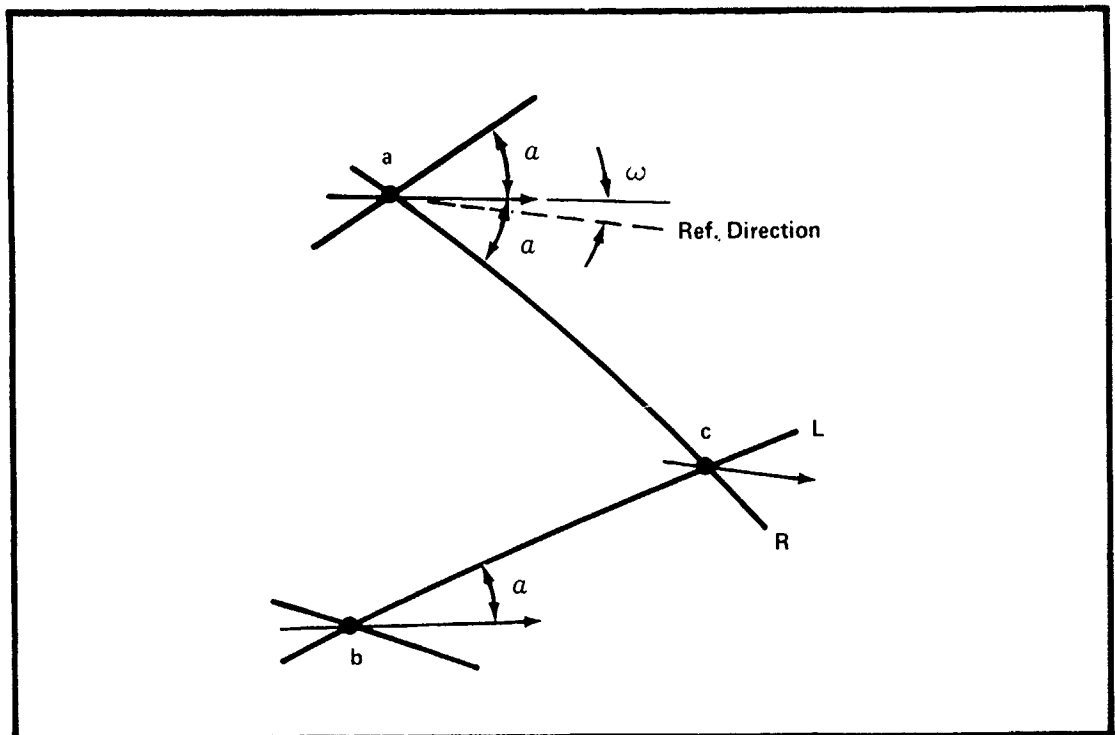


Figure 4. Conditions at c Are Determined by Characteristics for a and b

"Right-" and "left-running" characteristics are defined by the directions of the characteristics when viewed facing downstream. Assuming that points a and b supply the initial conditions, ie., their locations, as well as all flow properties, are known and a and b do not lie on the same characteristic, then a point c exists at the intersection of the left-characteristic (L) from b and the right-characteristic (R) from a. In a two-dimensional, conservative field, the location of c and the flow conditions at c may be determined. In terms of the direction of the flow

relative to the reference system, ω , and the Prandtl-Meyer function, $\nu(M, \gamma)$ two constants may be defined along the two characteristics through a given point,

$$R = \omega + \nu$$

and

3.2

$$L = \omega - \nu$$

thus for the point c,

$$\begin{aligned}\omega(c) - \nu(c) &= L(c) = L(b) = \omega(b) - \nu(b) \\ \omega(c) + \nu(c) &= R(c) = R(a) = \omega(a) + \nu(a)\end{aligned}$$

3.3

from which

$$\begin{aligned}\nu(c) &= 1/2 [\omega(a) + \nu(a) - \omega(b) + \nu(b)] \\ \omega(c) &= 1/2 [\omega(a) + \nu(a) + \omega(b) - \nu(b)]\end{aligned}$$

3.4

Although the Mach number, M , cannot be written explicitly as a function of the Prandtl-Meyer function, ν , it may be calculated by a method of successive approximations from the inverse functions $\nu = \nu(M)$; the particular technique used in this study is that in which each successive approximation is the average of the last two which bracketed the input, ν . Practically, an error of $\Delta M = 0.001$ is acceptable for most quantities derived from M , eg., pressure ratio, temperature ratio, etc., but for an accurate field solution the criterion should be an error increment in Mach angle

$$\alpha = \text{INV SIN} \left(\frac{1}{M} \right)$$

3.5

of $\Delta \alpha < 0.005^\circ$.

Locally, the characteristic is inclined at the Mach angle, α , to the velocity vector which, in turn, is inclined at ω to the reference frame. Thus the slope of an L-characteristic is $\tan(\omega + \alpha)$ and the slope of an R-characteristic is $\tan(\omega - \alpha)$. Point c may now be located by taking

mean slopes for linear segments between ac and bc (since $\alpha(c)$ and $\omega(c)$ as well as the values at a and b are now known. For bc the mean slope may be written as

$$S(bc) = \tan \left[\frac{\omega(b) + \omega(c)}{2} + \frac{\alpha(b) + \alpha(c)}{2} \right]$$

also

3.6

$$S(ac) = \tan \left[\frac{\omega(a) + \omega(c)}{2} - \frac{\alpha(a) + \alpha(c)}{2} \right]$$

Linear segments for bc and ac then give

$$X(c) = \left[Y(a) - Y(b) + S(bc) \cdot X(b) - S(ac) \cdot X(a) \right] \cdot \frac{1}{S(bc) - S(ac)}$$

3.7

$$Y(c) = Y(a) + S(ac) \cdot (X_c - X_a)$$

Thus from initial conditions at given points in the field, the interior may be solved within the characteristics from the extremities. It should be noted that the flow properties at intersections may be determined exactly but that the locations of the intersections depend upon the accuracy of the linear assumption for each segment. In practice, if the slope of a segment differed considerably from the preceding segment, then the segment should be subdivided and re-analyzed.

The procedures for determining the boundary locations are similar to those described above for characteristics. In Figure 4, if ac is a boundary streamline (free or solid) conditions at c can be determined by the left-characteristic constant and one of (1) a specified value of $\nu(c)$ if the boundary is free, (2) a value for $\omega(c)$ if the boundary is solid and specified or (3) a value for the constant $R(c)$ traced back to a specified zone. The equations become a set of special cases from those above: the slope for the linear segment ac is now

$$S(ac) = \tan \left(\frac{\omega(a) + \omega(c)}{2} \right) \text{ (Streamline)} \quad 3.8$$

The argument is similar if the boundary is replacing bc, rather than ac. Also, there is no difference if the field is being constructed in the upstream direction rather than the downstream direction.

In application, consider a Coanda jet nozzle discharging a supersonic flow with the upper boundary free and the other lower boundary solid, as sketched in Figure 5; in general, the flow through the nozzle exit af need not be uniform or parallel. If the flow through af is specified, then the flow downstream may be analyzed by constructing a characteristics grid in the manner described before. It follows that the shape of the boundary fh must be specified and the pressure distribution will be found. For the free boundary, the pressure distribution must be specified and its shape will be found. Note that a point g is influenced by both the nozzle exit distribution and the boundary fh .

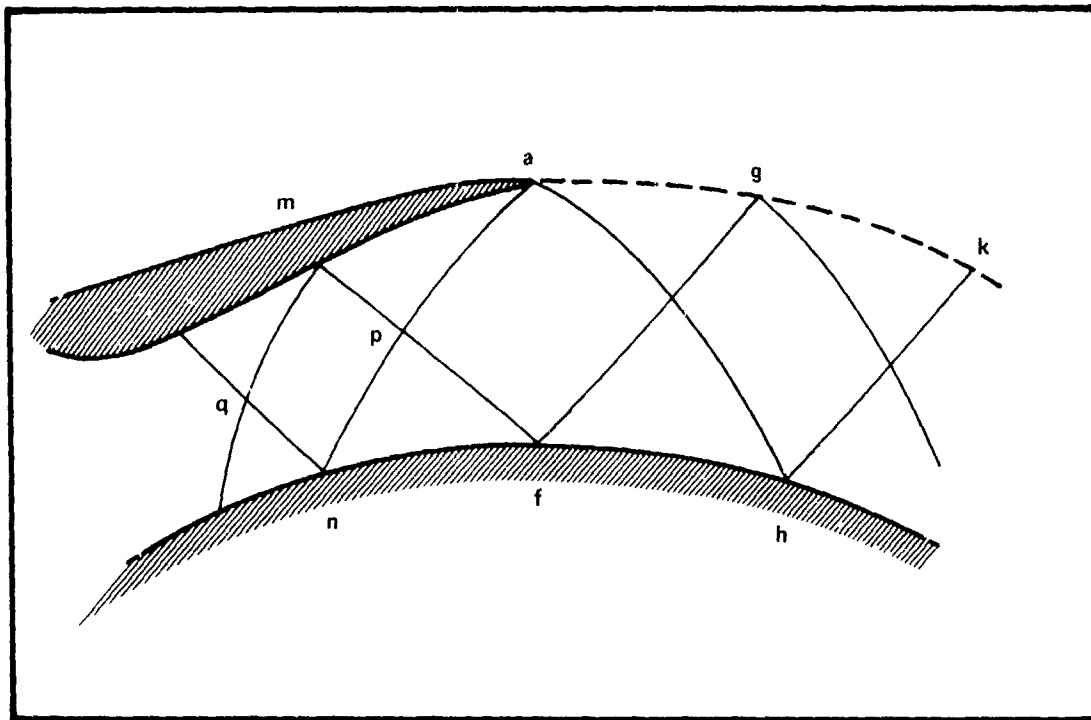


Figure 5. Schematic of Coanda Jet Characteristics

In practice, a more useful procedure would be to specify the exhaust flow by specifying the free boundary shape (and possibly the pressure distribution) and the solid wall shape. From these, the nozzle exit distribution could be calculated by an upstream running characteristics grid. The primary boundaries to be specified appear to be ag and fh ; however, it should be noted that conditions along fh are, in fact, determined by the free boundary segment, gk , as well as by the shape of fh . Thus, the desired nozzle flow is determined by specifying the shape of fh and the shape and pressure distribution along ak .

The internal contours for the nozzle which will deliver such a flow may be calculated by continuing an upstream-running characteristics solution. The shape of the zone afp and conditions at all points in that zone are fixed by the exit flow distribution; for points outside of and upstream from that zone the shape of the walls must be specified. Again, working upstream, it appears that a wide range of solutions is possible for the boundaries ma and nf within an implied assumption that the goal upstream is $M = 1$ (a throat). The approach developed by Guile yields one such solution. The procedure developed for this study will be described in the next section.

One-Step Design Approach

The one-step procedure may be described with reference to Figure 6. The flow field is visualized as consisting of cells bounded by direct and reflected characteristics from the specified exhaust flow between A and E . The region between point 2 and the exit AE is an expansion region for the flow. From the throat to point 4 is a conversion region for the throat, with the cell $4C\ 2G$ providing a match between the two.

As in all design procedures, there is a certain amount of trial and error. In solving the coarse net of Figure 6, the segments AB and FE are considered as "conditioning" the exhaust flow, i.e., of allowing a gradual

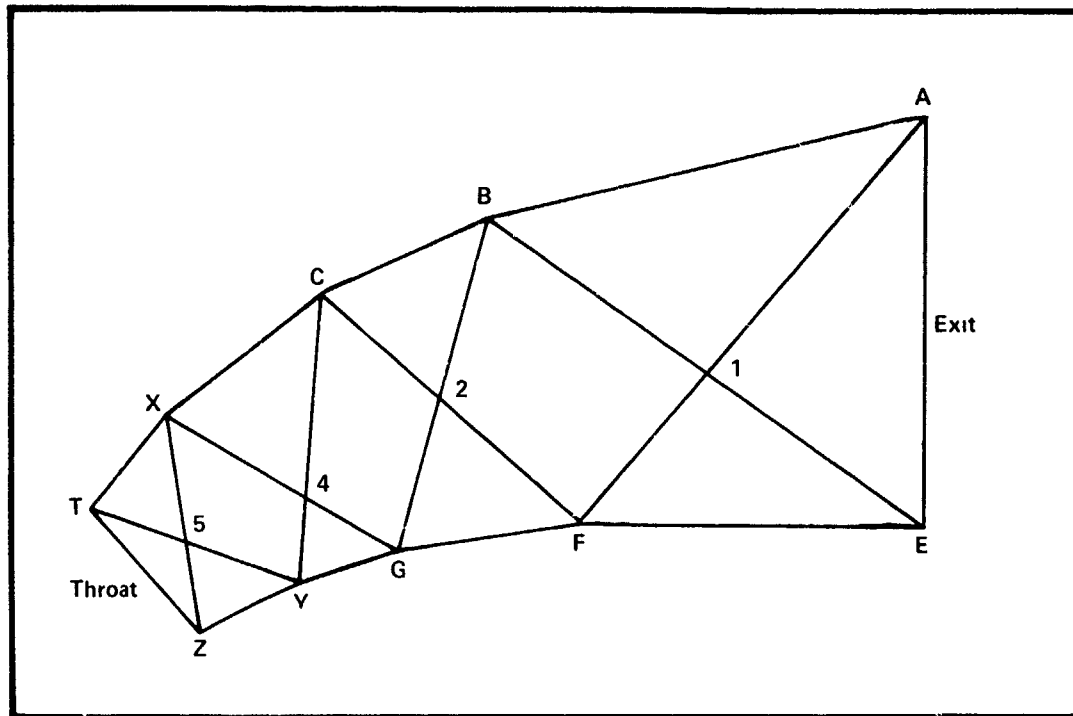


Figure 6. Coarse Net for the Nozzle Design Procedure

approach to the exhaust to avoid unusually high gradients, etc. Point 5 is specified as a throat condition (eg., $M = 1.001$), and the zones TX5 and ZY5 are specified as simple waves (single-family active characteristic) which must always bound a uniform flow zone. The selection of Mach number and flow directions at point 4 completes the coarse net specifications, which may now be analyzed for compatibility. For example, notice that point C may be related through point 2 to F and hence, to A and through point 4 to X and hence to 5. A "suitable" coarse net would have boundary Mach numbers increasing from throat to exhaust. If not, then another set of initial values could be tried. It is possible that the conditions in the exhaust distributions might be so extreme as to require the addition of another cell in the region between points 2 and 4.

With the acceptance of a coarse net, the nozzle flow may now be determined by a fine net. Starting at the nozzle exhaust flow and bounded by the specifications in the coarse net, a "characteristics operator" is

moved through the flow to the throat, determining the coordinates of the wall boundaries and the conditions (Mach number and flow direction) at each point. This is shown in Figure 7.

With conditions given at points 0 to 10, conditions at and locations of points 11 to 20 are found by the appropriate intersecting L- and R-characteristics; the procedure is repeated to find the next set (which are designated 1 to 9) and wall conditions are used to determine the points WU and WL on the respective upper and lower boundaries. The procedure is repeated and continued in the upstream direction in the same manner until the throat is reached.

The nozzle wall conditions are then examined in detail to insure that the Mach number is increasing in the downstream direction. If not, modifications are made to the coarse net and the procedure repeated until a satisfactory distribution is obtained.

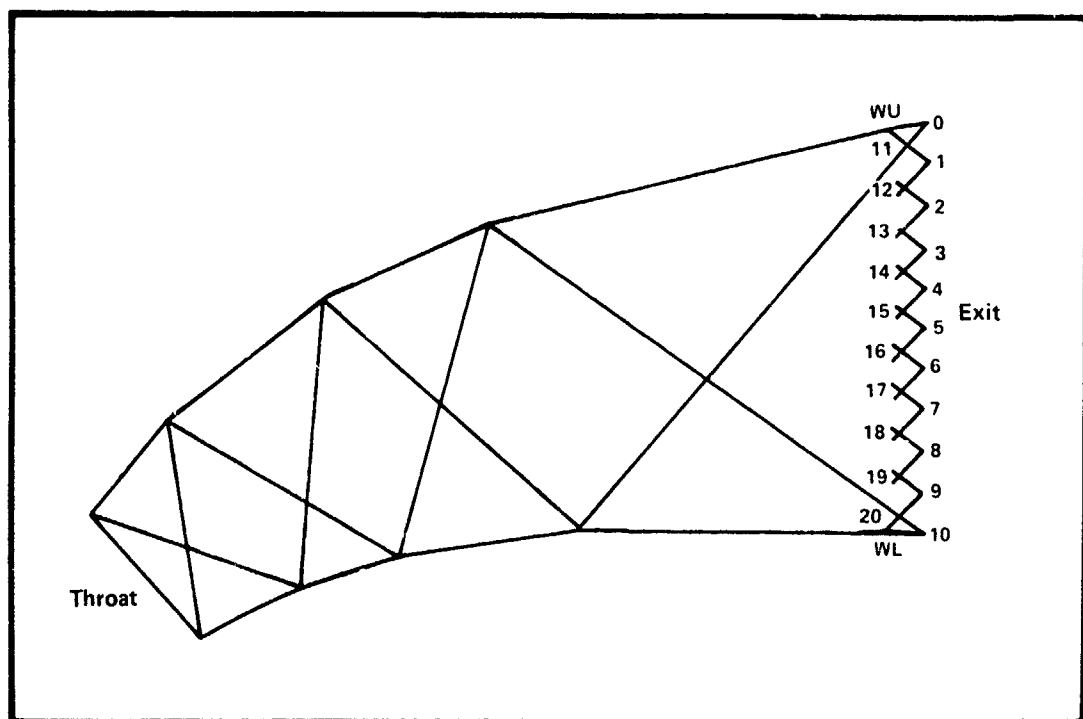


Figure 7. Fine Net Operator for the Nozzle Design Procedure

The next step in the design procedure is the calculation of the boundary layer displacement thickness. In this the method devised by Dayman¹⁴ was applied with a minor modification for a starting value at the throat because of the size of the actual device.

The throat starting-value was obtained by assuming a fully-turbulent flat plate at a Mach number of 0.5 for a distance equivalent to two nozzle heights. The resulting displacement thickness was "area-ratioed" to $M = 1$ and then Dayman's shape factor formula was used to obtain a starting value for the momentum thickness.

The steps taken in integrating along the nozzle were those defined by the end-points of the characteristics fine-mesh; this assumed that the surface slopes were everywhere so small that increments in X were an adequate approximation to increments in surface distance. At each step an increment in momentum thickness θ was calculated from

$$\frac{d\theta}{dX} = \frac{\rho C_f}{\mu} - \frac{dM}{dX} \left[\frac{2 - M^2 + H}{M(1 + 0.2M^2)} \right] \theta \quad 3.9$$

in which H is the profile shape factor, the ratio of the boundary layer displacement thickness to the momentum thickness. It was determined from the empirical relation:

$$H = 1.3 + 0.46M^2 \quad 3.10$$

The skin friction coefficient, C_f , was calculated from the empirical modification

$$\frac{C_f}{C_{f_i}} = (1 + 0.144M^2)^{-0.578} \quad 3.11$$

to the low speed Schultz-Grunom correlation for the incompressible skin friction coefficient,

$$C_{f_i} = \frac{0.0334}{(\log_{10} R\theta)^{1.838}} \quad 3.12$$

in which R_θ is the Reynolds number based on local flow conditions and local momentum thickness, ie.,

$$R_\theta = \frac{\rho V \theta}{\mu} \quad 3.13$$

Assuming ambient temperature as the stagnation value and the stagnation pressure as the design pressure ratio times atmospheric pressure, the local values for density, ρ , velocity, V , and viscosity, μ , were calculated from the local Mach number. Finally, the displacement thickness was calculated using the formula for H , above. The displacement thickness was added to the contour ordinates calculated for inviscid flow and then all were shifted so that the lower surface exit point was located at (0,0).

The computer program to perform the calculations was written in Basic language on a Radio Shack TRS-80; although the disk-based version of the language was used, the program is compatible with the lower version, Basic II. A line printer is called for to output, but in its absence, the program may be modified to give a CRT printout. Two versions were written, differing in the procedures to calculate Mach number from the Prandtl-Meyer function. $M = M(\nu)$ is not an analytic function so the inverse $\nu = \nu(M)$ is used in a half-internal search technique for one version termed "long." The "short" version, slightly less accurate, uses a polynomial fit to selected values for $M = M(\nu)$. The inviscid characteristics program can be used for any specific heat ratio input. The boundary layer analysis, however, is for an adiabatic airflow and would need modifications for gas flows much different from air and for large temperature differences between the gas and the nozzle wall.

The initializing input to the program includes the specific heat ratio, the design pressure ratio, and the inner Coanda radius ratio (radius divided by the height of the nozzle exit). The first phase of the program calculates the design Mach number of the outer streamline at

pressure equilibrium, the corresponding dimensionless velocity, the vortex constant, the velocity at 10 equally spaced points across the nozzle end and the corresponding Mach numbers. This information is displayed and if accepted, the program proceeds into the characteristics analysis. Certain features of the "conditioning" segments AB and EF are preset within the program according to experience and may be altered for special cases by trial and error. The values for the ambient atmospheric pressure and the supply temperature are also preset in the routine for the boundary layer and they may be reset for other situations.

Upon acceptance of the vortex distribution, the program proceeds with the coarse net analysis and requires some iterative input from the designer. When the results from the coarse net are acceptable to the designer, the program performs the flow analysis in fine mesh, starting with the initial 10 points across the nozzle exit. The results from the fine mesh analysis may be rejected in favor of a new start or accepted, in which case the boundary layer flow is then computed and the displacement thicknesses added to the contour coordinates.

For the design of a uniform flow nozzle, the preset condition for segments AB and EF should be altered to enforce symmetry or that cell may be skipped in the analysis. A uniform flow nozzle may be obtained by inputting a very large radius ratio, eg., 10^7 .

A listing of the program in the "long" form is presented in the Appendix.

Design of the Nozzles

The initializing mesh points and the starting profiles at the nozzle exit for the vortex nozzle and the uniform flow nozzle are given in Figure 8. The nozzles were designed to deliver these profiles. The same subsonic section was added to the upstream end of both nozzles.

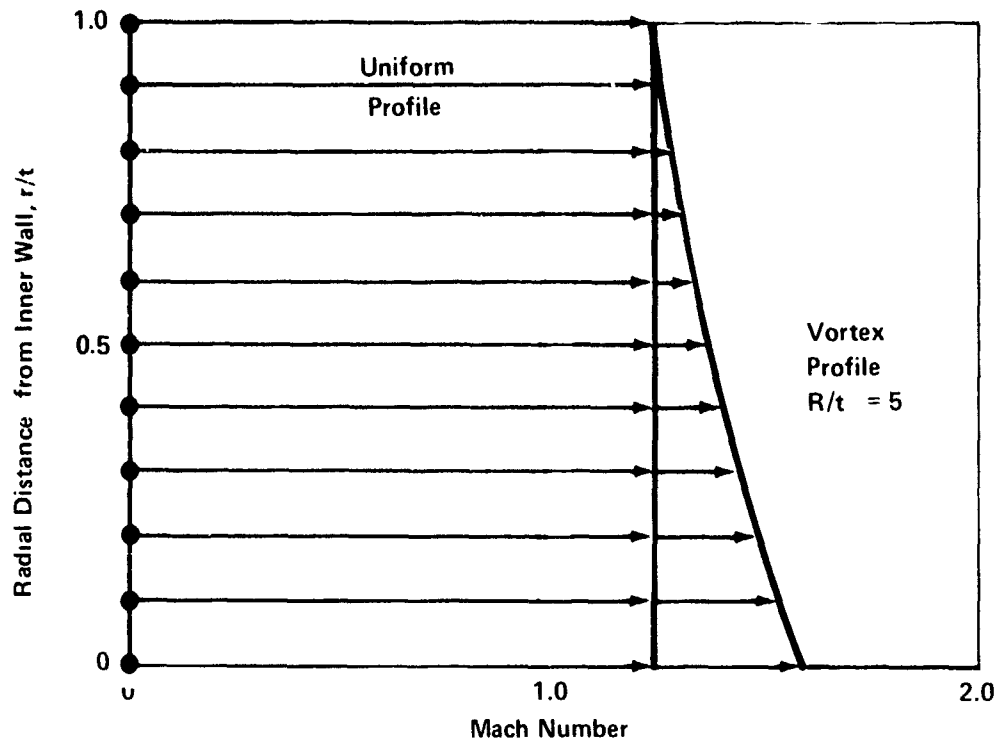


Figure 8. Exit Velocity Profiles for Which the Nozzles Were Designed

A design procedure that has been successful in delivering subsonic/transonic flows in wind tunnels at the OSU Aeronautical Research Laboratory was used to design these sections. The subsonic section is a simple cubic surface having both first and second derivatives going to zero at the throat.

Coordinates for the contours of both surfaces are given in the appendix; in those sets, the throat is indicated by a double point. Both nozzles are shown in Figure 9.

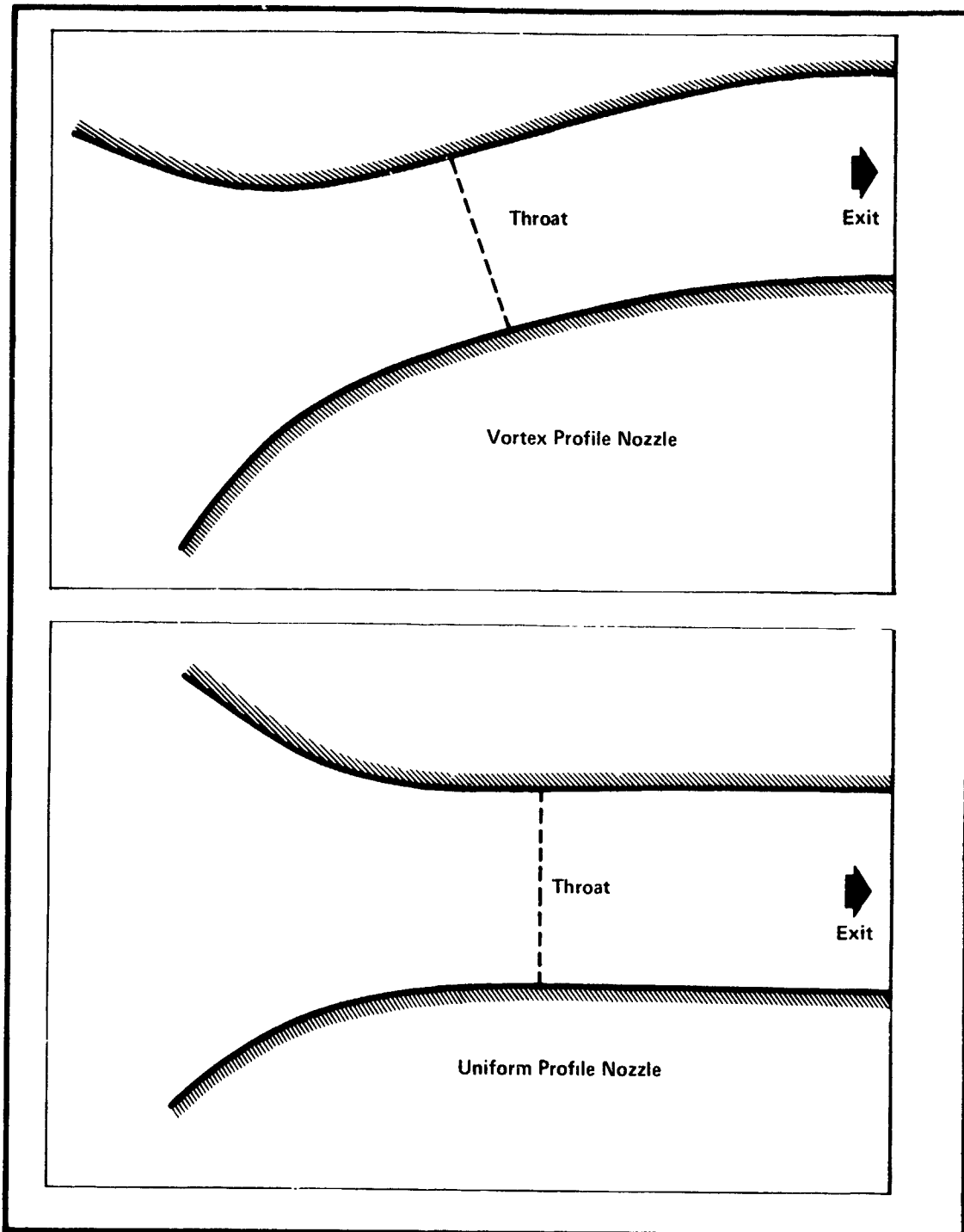


Figure 9. Contours of the Convergent-Divergent and Vortex Nozzles

SECTION IV EXPERIMENTAL APPARATUS

Description of the Model

The model consisted of a steel plenum box on which interchangeable nozzle and Coanda surface assemblies could be mounted, as shown in Figure 10. This plenum was attached to the balance post and was connected to the air supply hoses with two, four-inch pipes. A pressure tap in the plenum sidewall was used to measure the plenum pressure. Provisions were made to mount air distribution baffles in the plenum, but none were needed.

Both nozzle assemblies were nominally identical with the exception of the nozzle contours. Each assembly consisted of aluminum nozzle and Coanda surfaces mounted between steel endwalls. The nozzles had a span of 30.5 cm and nominal exit dimensions of 1.27 cm. The circular Coandas

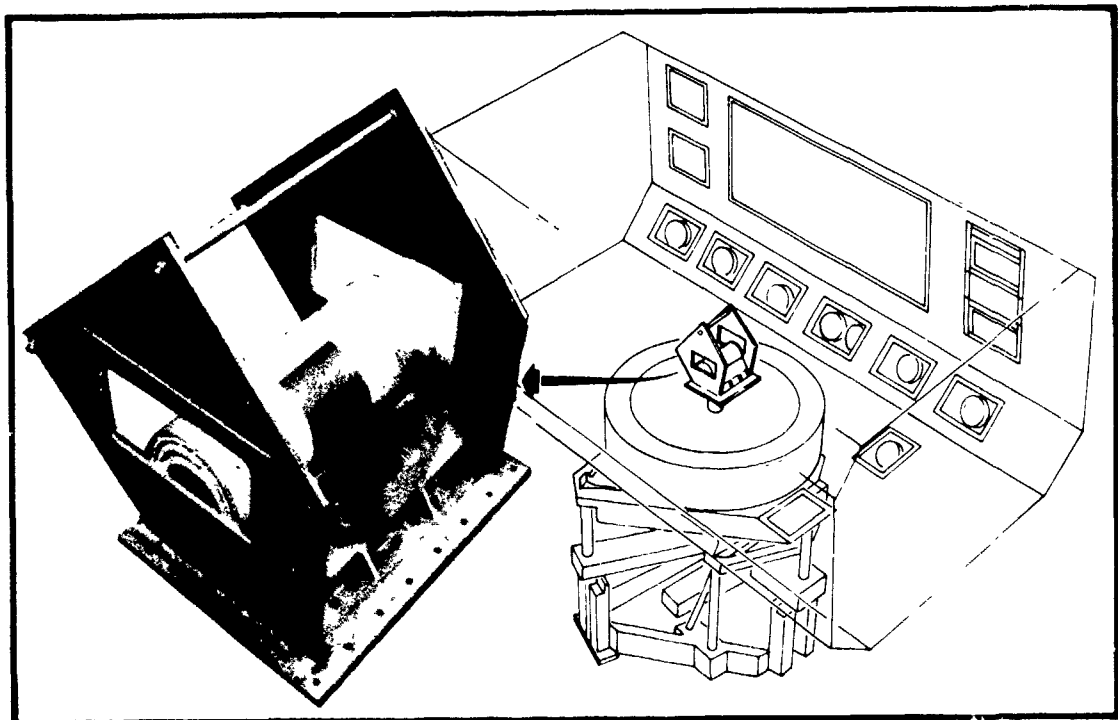


Figure 10. Vortex Turning Nozzle on 6-Component Balance

had a radius of 6.35 cm, giving $R/t = 5$. Both endwalls had openings which could be fitted with optical glass windows for flow visualization or with steel inserts for the force data runs. When the windows were not installed, the nozzle assembly was fitted with endwall boundary layer splitter plates. These splitter plates were 1.5 mm thick. These were mounted 1.27 cm and 2.54 cm from each endwall and were intended to insure the two dimensionality of the flow by removing the corner vortices. This technique was developed by Guitton & Newmann.¹⁵

The entire nozzle assembly was bolted to the plenum such that the nozzle exit plane was 45 degrees from the horizontal with the jet exhausting upward. Each nozzle assembly was instrumented with 15 pressure taps located on the inside nozzle contours and every 30° along the Coanda surface at midspan. Figure 11 shows the locations of these pressure taps.

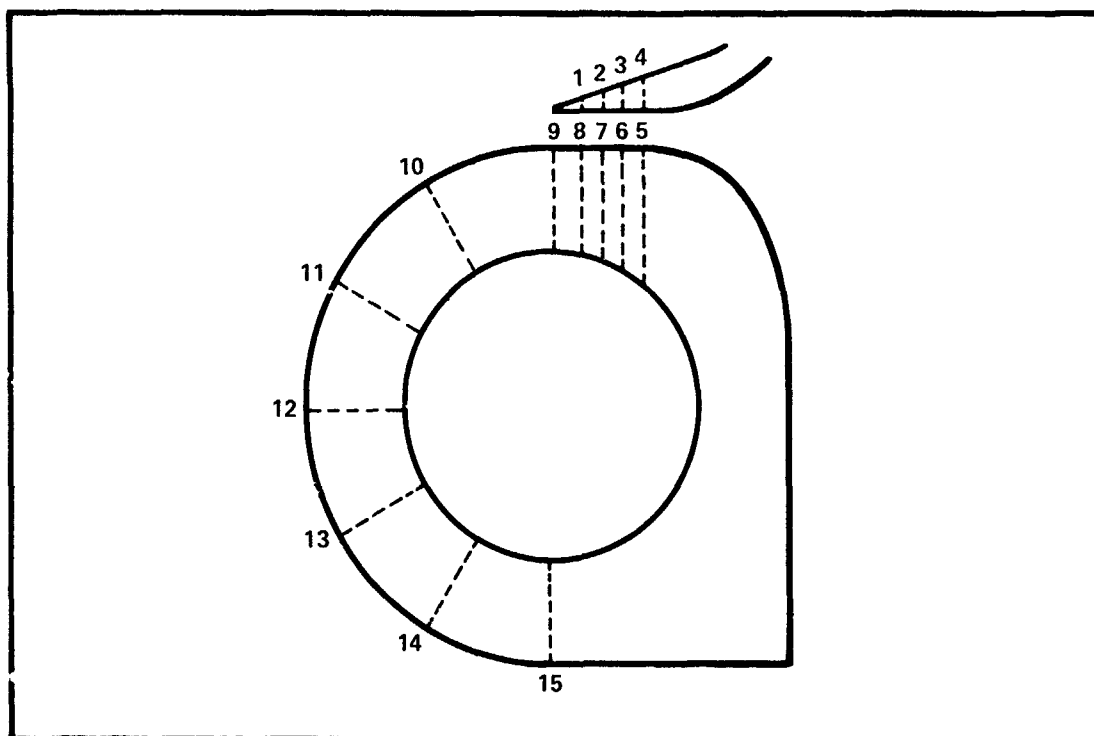


Figure 11. Location of the Pressure Taps on the Nozzle and Coanda Surface

The model was tested in the 7' x 10' test section of the NACAL low speed wind tunnel. The plenum was attached to a post connected to the six component external pyramidal balance. The model air supply was brought through two venturis and cono-flow control valves. Two 4-inch flexible hoses were used to bridge the balance with a minimum of interference.

Instrumentation

The following instrumentation was used to measure each nozzle's performance. All instrumentation was calibrated and read through the wind tunnel data system. Model forces were measured by the external six-component balance. The air supply mass flow was measured by two venturis in which the supply pressure, differential pressure and temperature were measured. The nozzle exit total pressure was calibrated versus the model plenum pressure which was obtained from the plenum wall static tap. Model surface pressures were recorded using a scanivalve. The air supply hose pressure was measured to be used for computing hose tares. The above instrumentation was recorded and reduced by an IBM 1800 data acquisition computer. Nozzle exit and jet profile survey data were acquired on an x-y recorder using a pressure transducer and a calibrated traverse position potentiometer.

SECTION V

RESULTS AND DISCUSSION

Force Balance Measurements

A straightforward comparison of the magnitude and direction of the thrust vector was used to evaluate the turning efficiency of the two nozzles. These quantities were determined from the force balance data. Surface pressure distributions, dynamic pressure profiles, and Schlieren photographs were also obtained in order to interpret the basic force data. The variation of the thrust deflection angle with the nozzle pressure ratio (the ratio of the jet stagnation pressure to the ambient pressure) is shown in Figure 12. These angles were computed from the measured vertical and horizontal components of the force, according to the relation

$$\phi_{\text{def}} = 225^\circ - \tan^{-1} (F_y/F_x) \quad 5.1$$

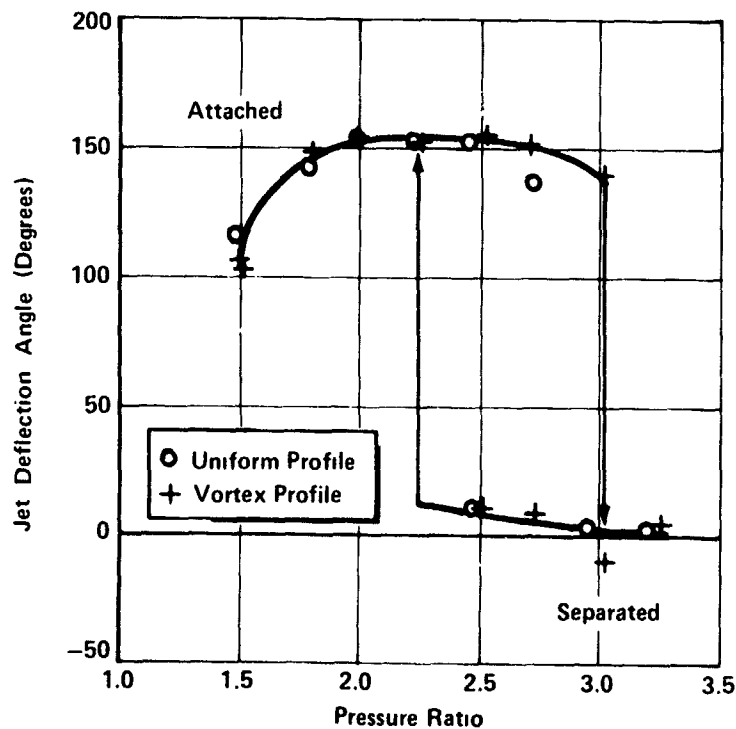


Figure 12. Variation of Jet Turning Angle with Nozzle Pressure Ratio

which gives the deflection relative to the nozzle axis. This thrust deflection angle is not the same as the jet separation angle, because the mixing of the jet with the surrounding fluid causes the outer jet boundary to turn more slowly than the inner boundary. As a result, the thrust vector is not tangent to the surface at the separation point.

In the figure it can be seen that for the range of pressure ratios between 2.2 and 3.0, the attachment of the jet shows some hysteresis; that is, the jet remains attached if the pressure ratio is increased through this range, and the jet remains separated if the pressure is decreased through the range. The surprising result of these measurements is the size of the angle through which both jets were deflected. The maximum deflection of almost 155° was obtained up to the design pressure ratio of 2.5. In fact, the turning of both jets was probably limited by interaction with the nozzle plenum on the back side of the Coanda surface.

The deflection of the two jets was the same. Up to the design pressure ratio the deflection of both jets increased with the pressure ratio. As the pressure ratio was further increased, the jet deflection decreased slightly, until sudden detachment occurred at $PR \sim 3.0$. The jets deflected slightly as the pressure ratio was then reduced below the design value, until sudden re-attachment occurred at $PR \sim 2.25$.

The variation in the jet thrust coefficient is shown in Figure 13. The coefficient is defined as the ratio of the jet thrust measured on the force balance,

$$T = (F_x^2 + F_y^2)^{1/2} \quad 5.2$$

to the thrust calculated for an isentropic expansion of the measured nozzle mass flow to atmospheric pressure. This is the same as the definition of nozzle velocity coefficient. However, the presence of the Coanda surface affects the measured thrust. When the jets are attached, the thrust is

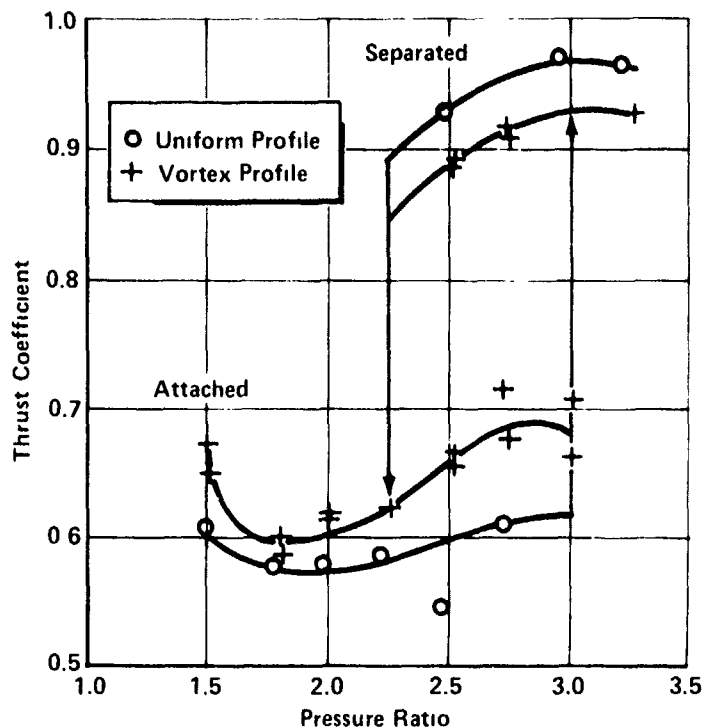


Figure 13. Variation of Jet Turning Efficiency with Nozzle Pressure Ratio

reduced by wall friction and when the jets are detached, the thrust is reduced by suction forces on the Coanda surface.

The measured variation of the thrust coefficient is consistent with the observed deflection of the jet. Initially, as the pressure ratio and deflection increase, the thrust is reduced. Then, as the pressure ratio was increased past the design value and the deflection decreased, the thrust increased. After separation, the thrust decreased with pressure ratio, as the jet deflection increased.

Although the error in these measurements is on the order of 5%, the consistent difference in the thrust coefficient of these jets does suggest that the vortex nozzle increases the thrust of the deflected jet and would thus be more effective in a thrust vectoring system. On the other hand, the separated jet from the vortex nozzle may have less thrust than

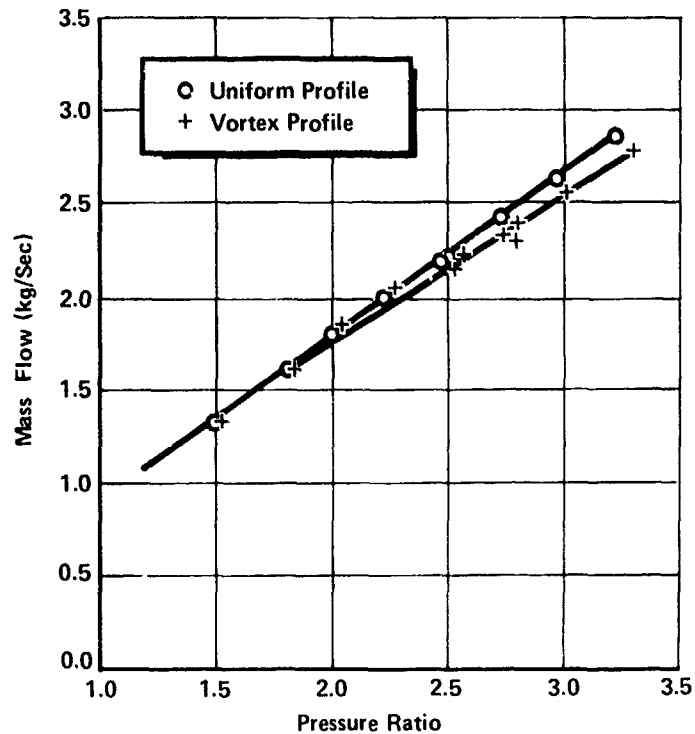


Figure 14. Variation of Jet Mass Flow with Nozzle Pressure Ratio

the jet from the convergent-divergent nozzle. As a point of comparison, the jet from a simple convergent nozzle, tested on the same model, separated at a $PR \sim 2.65$ and re-attached at a $PR \sim 2.0$. The thrust and deflection of the attached jet was similar to that of the other jets.

The measured mass flow of the two convergent-divergent nozzles is compared in Figure 14. Since both were designed with the same throat dimension, they would be expected to have the same mass flow.

Surface Pressure Measurements

The static pressure distributions measured within the nozzle and on the Coanda surface at the design PR are shown in Figures 15 and 16. In both figures the nozzle exit is at the top. There are five equally spaced taps between the throat and the exit of each nozzle, and a tap

every 30° along the Coanda surface. The general shape of the measured pressure distributions are similar for both nozzles. As the flow expands through the nozzle, the pressure decreases to atmospheric pressure. Then, as the jet is turned onto the Coanda surface, the pressure drops well below atmospheric pressure. Viscous effects then cause it to increase again.

The pressure on the upper wall of the convergent-divergent nozzle decreases smoothly to atmospheric pressure, as expected. On the lower wall, however, the pressure at the exit is already below atmospheric pressure as seen in Figure 15. This may be due to the formation of a separation bubble, which develops because the jet first resists turning, then re-attaches further downstream.

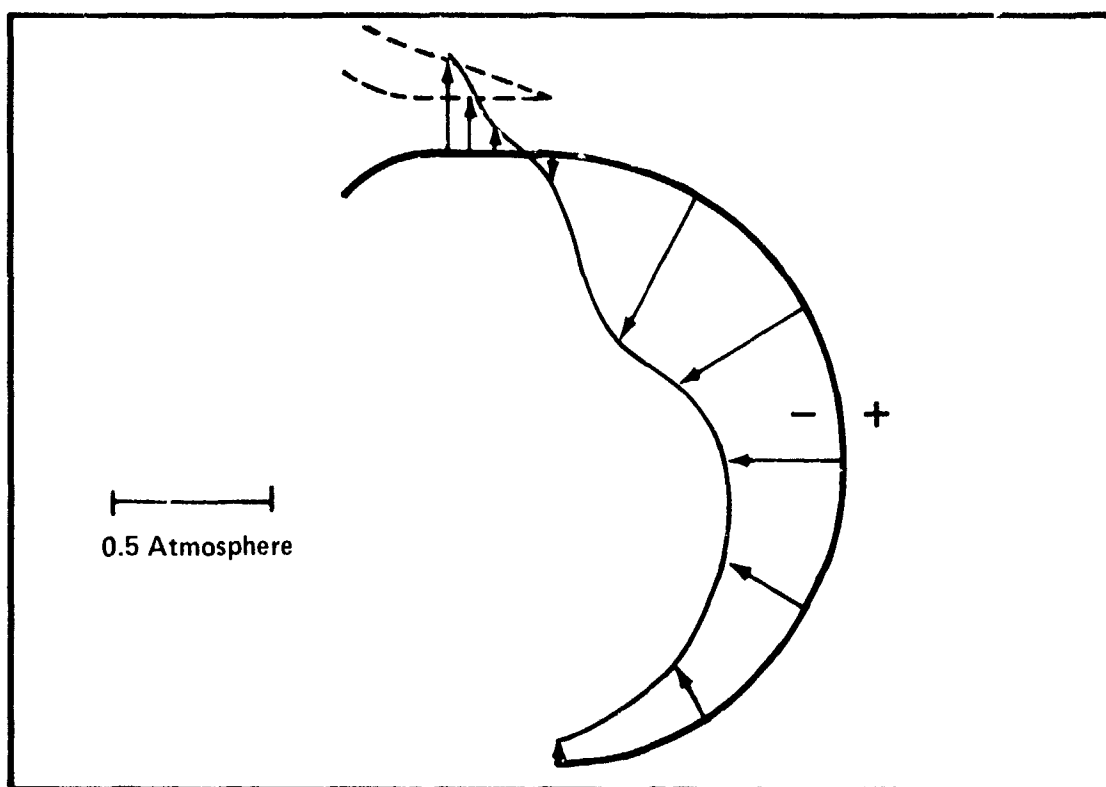


Figure 15. Static Pressure Difference $(P - P_\infty)$ over the Convergent-Divergent Nozzle

The surface pressure under the Coanda jet can be estimated with Equation 2.3. The jet thrust was calculated from the measured mass flow, \dot{m} , and the nozzle pressure ratio, according to the relation,

$$T = \dot{m} \left[\frac{2\gamma}{\gamma-1} RT_0 \left(1 - (P_\infty/P_0)^{1/\gamma} \right) \right]^{1/2} \quad 5.3$$

in which R is the gas constant, while P_0 and T_0 are the stagnation pressure and temperature. At the design pressure ratio, the thrust of the jet is about 27 newtons/cm of span, and the pressure drop is 0.39 atmospheres. The maximum pressure drop on the Coanda surface (at $\phi = 30^\circ$) is slightly less than this.

The vortex nozzle pressures shown in Figure 16 are more difficult to interpret. The pressure on the inner wall of nozzle decreases more

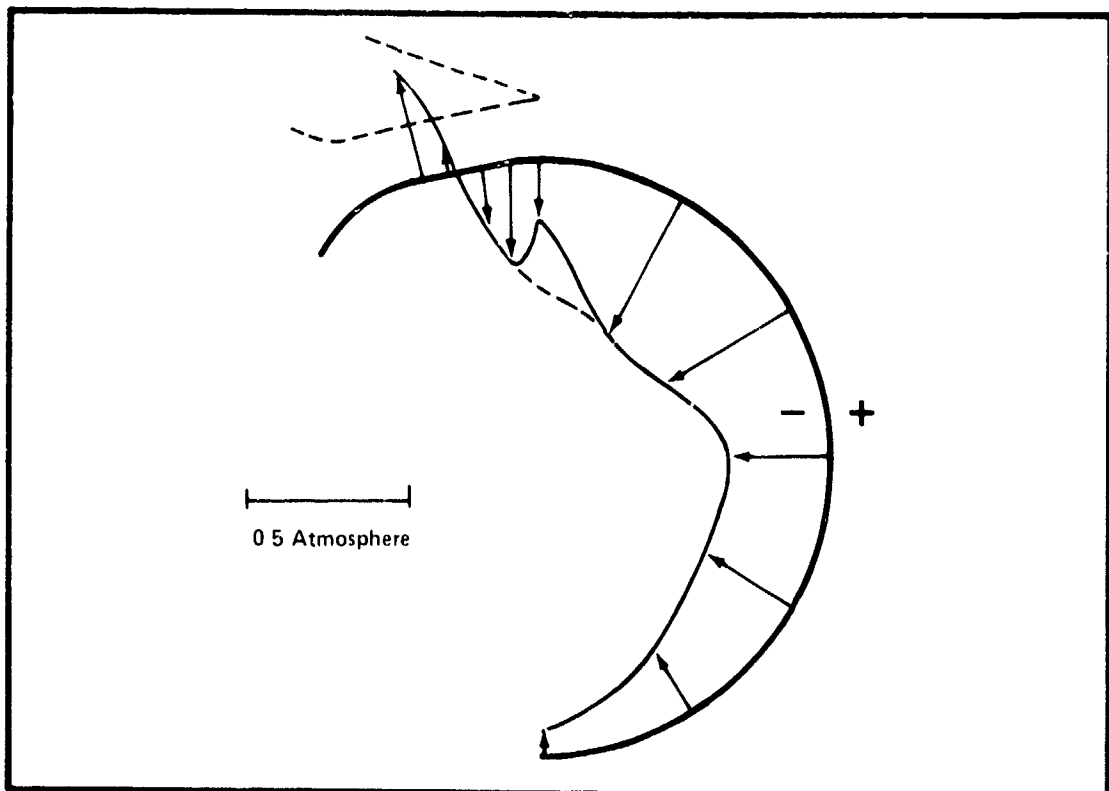


Figure 16. Static Pressure Difference ($P-P_\infty$) over the Vortex Nozzle

rapidly than in the conventional nozzle, and approaches the value required to turn the jet. However, the pressure rises at the nozzle exit, before decreasing again on the Coanda surface. There is a similar pressure rise on the upper wall of the nozzle. Since these taps show similar behavior at subsonic pressure ratios, it is likely they are defective, but it is also possible that a compression wave originates on the upper surface of the nozzle and impinges further downstream on the lower surface. Examination of these taps did not reveal any defects so that it was not possible to resolve this question.

In Figures 17 and 18 the measured nozzle wall pressures are compared to the predicted pressure distributions. Except for the taps previously noted, the agreement is very good. There is a region on the upper wall of the vortex nozzle where the pressure gradient is relatively flat so

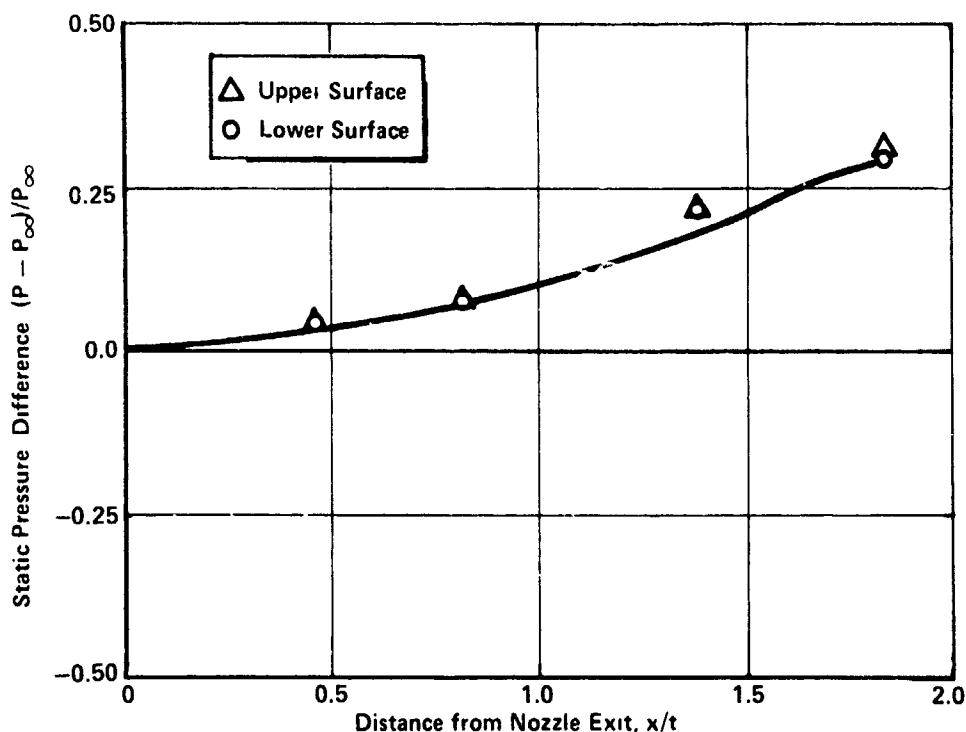


Figure 17. Comparison of Predicted and Measured Pressures in the Conventional Nozzle

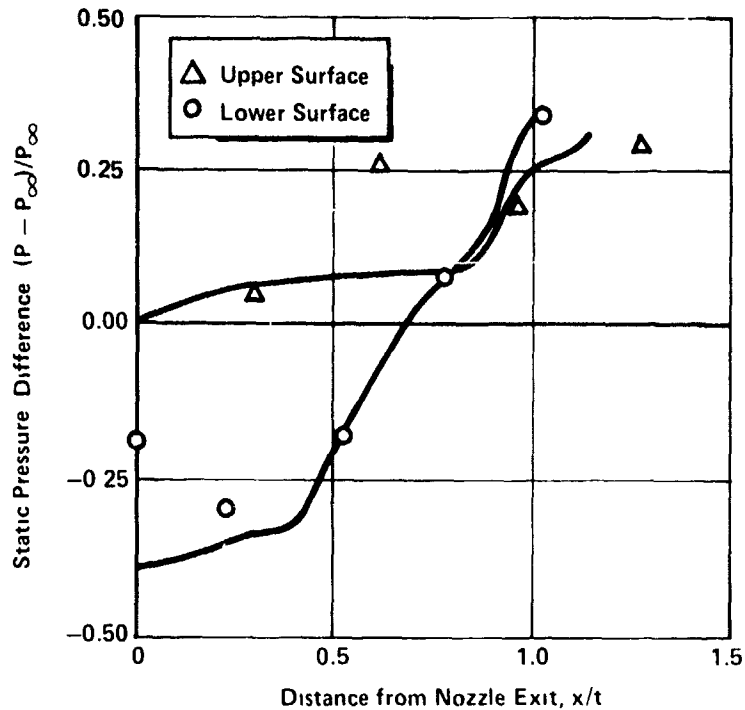


Figure 18. Comparison of Predicted and Measured Pressures in the Vortex Nozzle

that a compression wave may have formed here. However, the correct pressure at the downstream tap suggests that the wave, if it exists, must be relatively weak, and the measured total pressure profiles at the nozzle exit indicate that a vortex-like profile was delivered by the nozzle.

Total Pressure Profiles

Jet total pressure profiles were measured at the nozzle exit and along the Coanda surface over each of the static pressure taps. These were used to compare the spreading of the jets. In Figure 19, the total pressure profile at the exit of the vortex nozzle is compared to the predicted distribution. This distribution was calculated from the computed velocity profile. Since the local Mach number is higher near the inner wall, the pressure loss due to the probe shock is larger there. Thus, the slope of the total pressure profile is opposite to the slope of the velocity profile.

The agreement is very good, except near the inner wall, where there is a spike which may be due to boundary layer separation induced by the probe or by the suspected compression wave. The fact that similar spikes are seen in the conventional nozzle suggests that probe interference may be at fault.

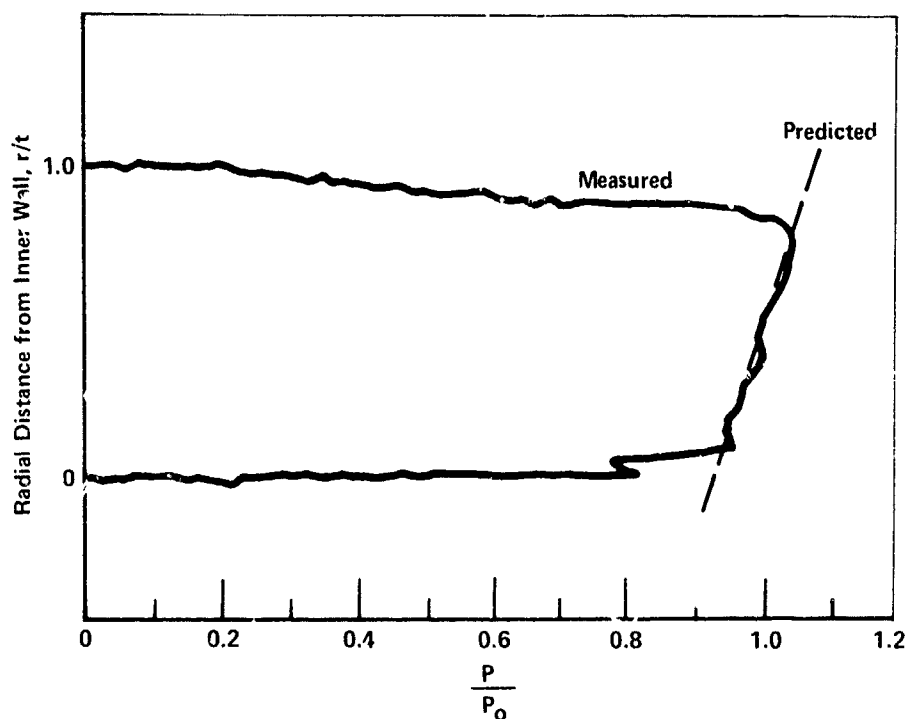


Figure 19. Predicted and Measured Total Pressure Profiles at the Exit of the Vortex Nozzle

The spreading of the jets is shown by the development of the total pressure profiles in Figures 20 and 21. Both jets develop in the same way. The inner boundary layer and the outer mixing layer have merged by the 30° station to form the pressure profile typical of wall jets. However, the spreading of these jets is considerably more rapid than that of a wall jet on a flat plate. It is worth observing that the jet from the vortex nozzle spreads noticeably faster than the jet from the conventional nozzle. The reasons for this behavior are not known.

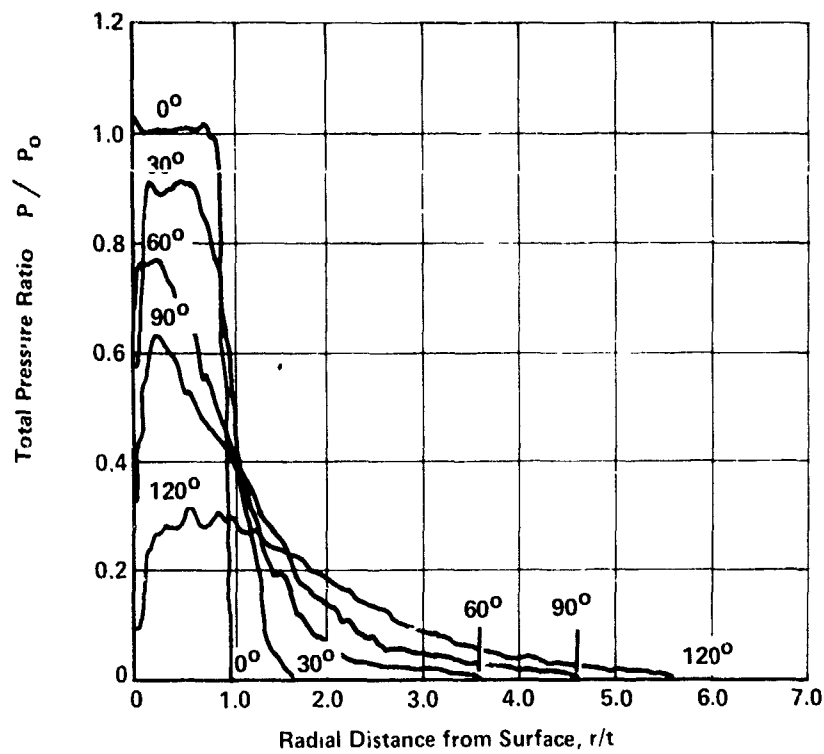


Figure 20. Development of the Total Pressure Profiles from the Conventional Nozzle

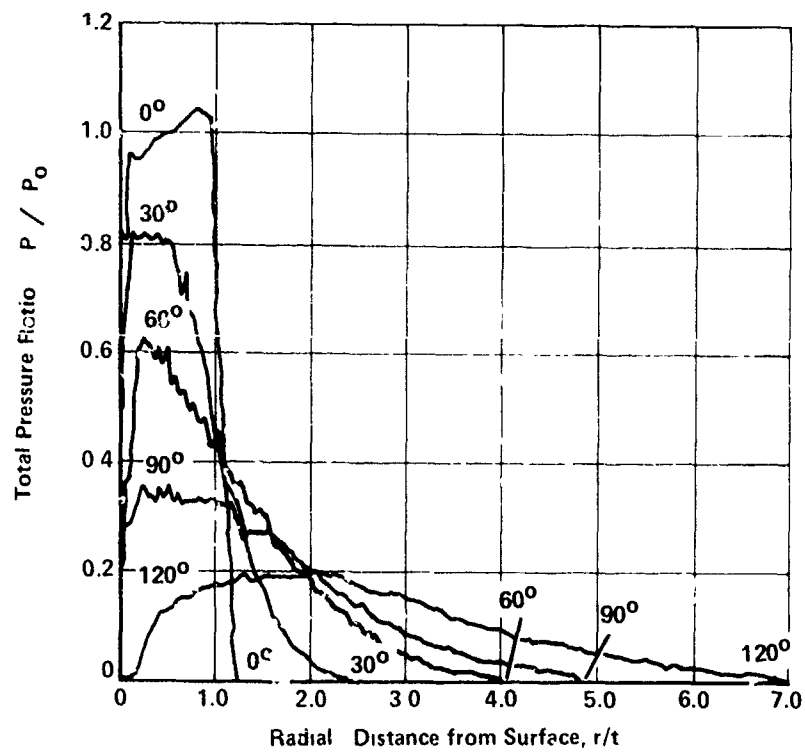


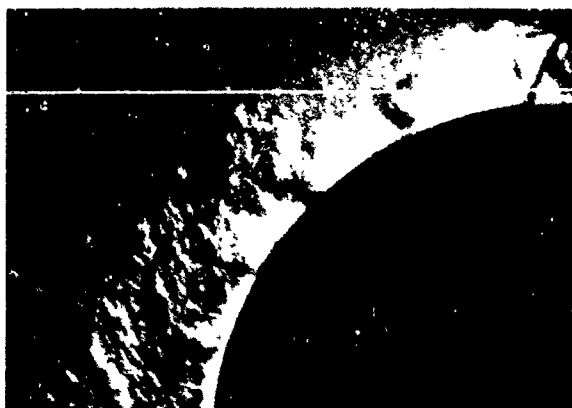
Figure 21. Development of the Total Pressure Profiles from the Vortex Nozzle

Schlieren Photographs

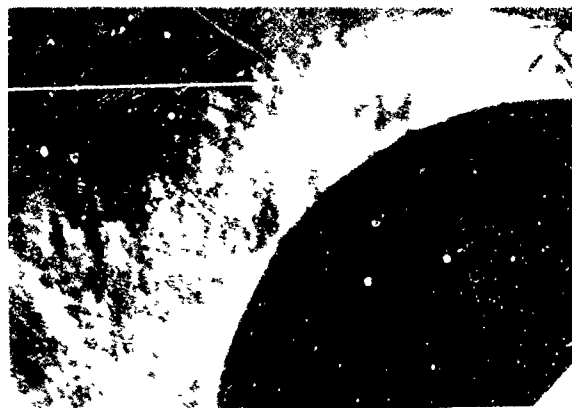
As a further aid in understanding the behavior of these jets, Schlieren photographs were made of the region downstream of the nozzle exit. A representative series of these photographs are shown for each of the three nozzles in Figures 22 through 24. These include a photograph of each jet at the design pressure ratio, at the pressure ratio for detachment, and at the pressure ratio for re-attachment.

In the photographs it can be seen that the detachment of each jet is caused by shock induced boundary layer separation. This occurs when the wave system in the jet becomes strong enough to cause separation of the jet boundary layer. The orientation of the Schlieren system is such that the compression wave reflected from the wall and the separation bubble behind it are made visible in the photographs of the jets before detachment. When the boundary layer does separate, the jet is deflected away from the wall. This strengthens the shock and moves the separation point upstream. The separation point of the detached jet is therefore closer to the nozzle than the initial point of separation. The slight deflection of each jet before re-attaching, which was observed in the balance data, is also apparent in the photographs.

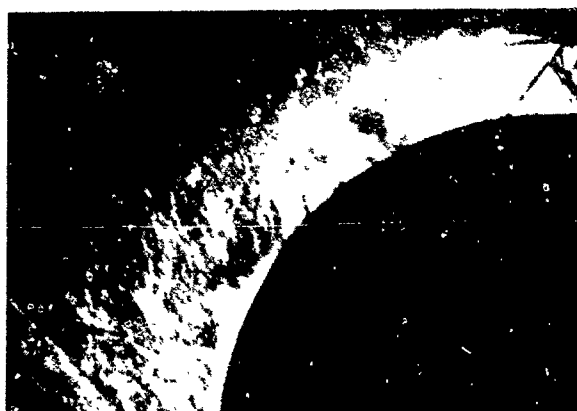
The reasons for the differences in the jet detachment behavior may be deduced from these photographs. All three jets are attached at the design pressure ratio. This ratio was chosen on the basis of difficulty previously^{2,9} reported in achieving attachment with convergent nozzles for these conditions. In fact, the convergent nozzle did separate at a slightly higher pressure ratio, and could be made to separate at lower pressures by introducing a disturbance into the jet. Thus, the behavior of this jet is consistent with the limited data available, and it may be concluded that the expansion waves reinforced the turning wave and cause detachment at a low pressure ratio in this case.



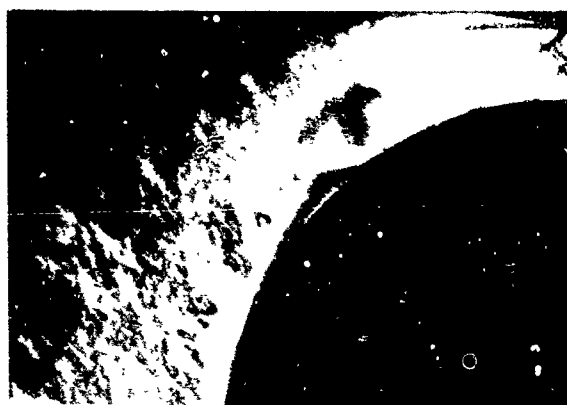
PR~2.0



PR~2.5 DESIGN POINT



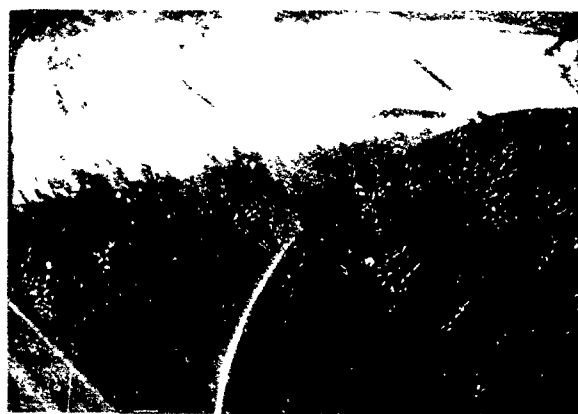
PR~2.25 AFTER REATTACHMENT



PR~3.0 BEFORE DETACHMENT



PR~2.25 BEFORE REATTACHMENT



PR~3.0 AFTER DETACHMENT

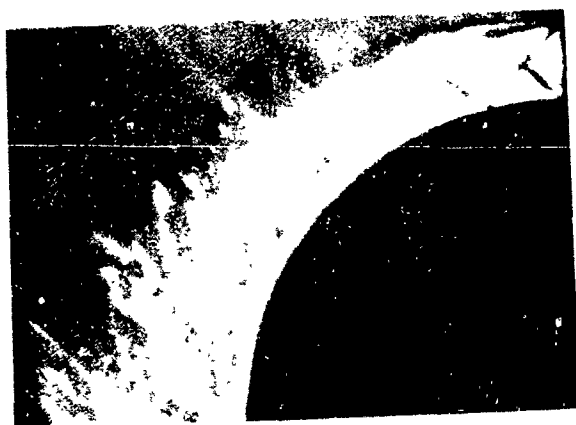
Figure 22. Schlieren Photographs of the Coanda Jets from the Convergent Divergent Nozzle



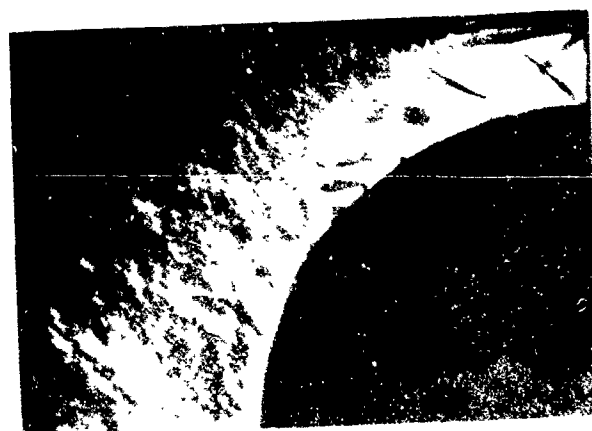
PR~2.0



PR~2.5 DESIGN POINT



PR~2.25 AFTER REATTACHMENT



PR~2.8 BEFORE DETACHMENT



PR~2.25 BEFORE REATTACHMENT

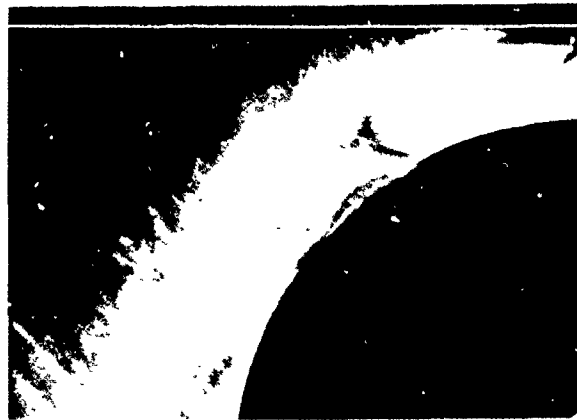


PR~3.0 AFTER DETACHMENT

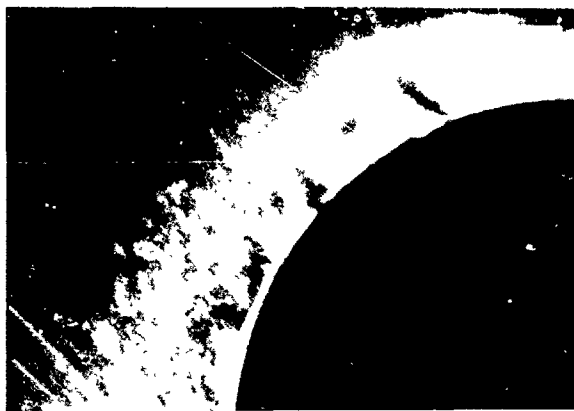
Figure 23 Schlieren Photographs of the Coanda Jets from the Vortex Profile Nozzle



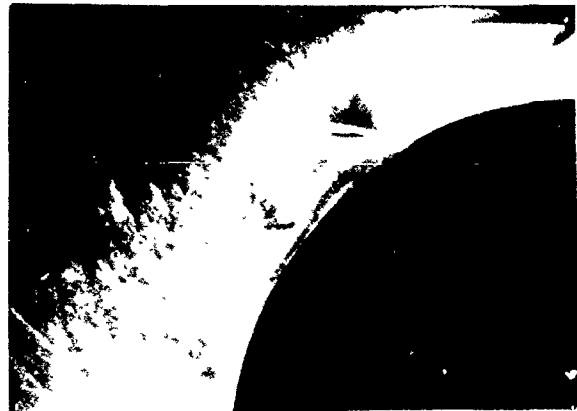
PR ~ 2.25



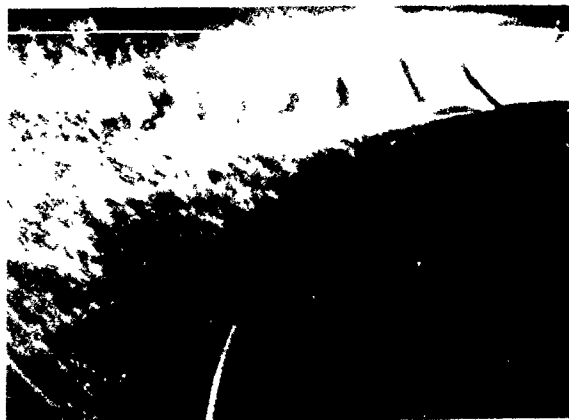
PR ~ 2.5 ATTACHED



PR ~ 2.0 AFTER REATTACHMENT



PR ~ 2.65 BEFORE DETACHMENT



PR ~ 2.0 BEFORE REATTACHMENT



PR ~ 2.65 AFTER DETACHMENT

Figure 24 Schlieren Photographs of the Coanda Jet from the Converging Nozzle

The convergent-divertent nozzle did not detach at a lower pressure than the vortex nozzle, because the turning waves, by themselves, were not strong enough to cause detachment at the design pressure ratio. Both of these convergent-divergent nozzles therefore separated at the same pressure ratio, when the expansion wave system became strong enough. On this basis, the jet from a vortex nozzle may be expected to remain attached at higher pressure ratios and for smaller radius surfaces, when the turning shocks would detach the jet from a simple convergent-divergent nozzle.

SECTION VI

CONCLUSIONS

Several important conclusions about the thrust vectoring of Coanda jets can be drawn from this study. First, the turning of supersonic Coanda jets is greatly improved by the use of convergent-divergent(C-D) nozzles, rather than simple convergent nozzles. This is because the expansion waves at the exit of a convergent nozzle cause it to separate at a relatively low Mach number. C-D nozzles provide better turning in the transonic regime also, because the effect of curvature is to lower the pressure on the wall at the nozzle exit and produce regions of locally supersonic flow.

Although the vortex profile nozzle did not produce greater turning than the conventional C-D nozzle for the radius and pressure ratios investigated, the turning of both nozzles was much better than for a convergent nozzle. In addition, the thrust of the deflected jet was 6% to 11% greater than that of the conventional C-D nozzle. Although the turning shocks were too weak to separate the conventional jet in these tests, the vortex nozzle may still provide better turning at higher pressure ratios or for tighter radius turns. This possibility should be investigated.

An improved nozzle design procedure, which results in a shorter and lighter vortex profile nozzle was also developed as part of this study. This procedure may also be useful for reducing the length of the vortex nozzles used to generate aerodynamic windows for gas dynamic lasers.

APPENDIX A

```

5 REM DESIGN PROGRAM FOR COANDA NOZZLE
10 DIM X(20), Y(20), N(21), D(20), W(21), R(20), L(20), L(20), XU(40),
    YU(40), XL(40), YL(40), NU(40), NL(40), DU(40), DL(40), WU(40),
    WL(40), X1(20), Y1(20), D1(20), W1(20), N1(20), L1(20), R1(20),
    X2(20), Y2(20), D2(20), W2(20), N2(20), R2(20), L2(20), YT(40),
    YB(40), SU(40), SL(40)
12 PI = 3.14159
15 INPUT "SPECIFIC HEAT RATIO:" G:G1 = (G + 1)/(G - 1): G2 = SQR(G1):
    G3 = G/(G - 1):G4 = 1/G3
25 INPUT "EXHAUST PRESSURE RATIO:" PR:MA = SQR ((PR G4 - 1)*2/(G - 1):
    PRINT""OUTER EDGE MACH NO IS"; MA
35 VI = 1/SQR(2/G + 1)/MA/MA + 1/G1)
40 PRINT "ENTER INNER RADIUS AS A MULTIPLE OF NOZZLE EXIT HEIGHT": INPUT
    ER: ER = ER*10:KI = VI*(ER + 10)
41 LPRINTCHR$(14)" ":LPRINTCHR$(30) "NOZZLE DESIGN OUTPUT FROM":LPRINTCHR
    $(31)" ":LPRINT" COANDA 7":LPRINTCHR$(31)"REV 5 SEPT 79":LPRINTCHR$(30)"
    ":LPRINT" ":LPRINT"SPECIFIC HEAT RATIO = ":G
43 LPRINT"PRESSURE RATIO = ":PR:LPRINT" INNER RADIUS RATIO (TO NOZZLE)
    = ":ER/10:LPRINT" "
45 LPRINT" ":LPRINT"INITIAL DISTRIBUTION":LPRINT" ":LPRINT"Y", "MACH NO"
    :LPRINT" "
50 FOR I = 0 TO 10:Y(I) = 10 - I:X(I) = 0:D(I) = 0:VS = KI/(Y(I) + ER):
    M = 1/SQR((G + 1)/2/VS/VS - (G - 1)/2):N(I) = G2*ATN(SQR(M*M - 1)/
    G2) - ATN(SQR(M*M - 1)):W(I) = ATN(1/SQR(M*M - 1)):R(I) = N(I):L(I)
    = N(I):LPRINTY(I), M:NEXTI:WL(0) = ATN(1/SQR(M*M - 1)):LPRINTCHR$(29)""
80 XU(0) = 0:YU(0) = 10:XL(0) = 0:YL(0) = 0:DU(0) = 0:DL(0) = 0:NA = N(0):
    WA = W(0):DA = D(0):WU(0) = WA:WE = W(10):WL(0) = W(10):NE = N(10):
    DE = D(10):ME = 1/SIN(WE)
85 NU(0) = NA:NL(0) = NE
90 FORI = 0 TO 20:X1(I) = X(I):Y1(I) = Y(I):D1(I) = D(I):N1(I) = N(I):
    W1(I) = W(I):R1(I) = R(I):L1(I) = L(I):NEXTI
100 REM POLY FOR M(N)

```

```

110 P = 1/3:M = 1.01:SQ = SQR(M*M - 1):N8 = G2*ATN(SQ/G2) - ATN(SQ):
    Q8 = PI/2 - STN(1/SQ):SQ = SQR (ME*ME - 1):N9 = G2*ATN(SQ/G2) - ATN
    (SQ):Q9 = PI/2 .. ATN(1/SQ)
120 00 = (Q9/N9↑.9-Q8/N8↑.9)/(N9↑(P - .9) - N8↑(P - .9)):01 = Q9/N9↑
    .9 - 00*N9↑(P - .9)
150 REM COARSE NET
155 CLS:PRINT "ANALYSIS OF NOZZLE BY COARSE NET"
157 MB = .95*MA:MF = .95*ME:SQ = SQR(MB*MB - 1):NB = G2*ATN(SQ/G2) - ATN
    (SQ):SQ = SQR(MF*MF - 1):NF = G2*ATN(SQ/G2) - ATN(SQ)
160 N1 = (NA + DA + NE - DE)/2:D1 = (NA + DA - NE + DE)/2:W = PI/2 - 00*
    N1↑P - 01*N1↑.9:M1 = 1/SIN(W):DB = NB - N1 + D1:DF = N1 + D1 - NF:
    N2 = (NB + DB + NF - DF)/2:D2 = (NB + DB - NF + DF)/2:W = PI/2 - 00*
    N2↑P - 01*N2↑.9:M2 = 1/SIN(W)
165 PRINT"M1 = ";M1, "D1 = ";D1:PRINT"FRIST SEGMENT IS TRANSITION FOR
    BOTH SURFACES":PRINT"MB = ";MB, "MF = ";MF:PRINT" M2 = ";M2," D2:
    PRINT," (ON ERROR GO TO 5115 OR 1060)"
170 INPUT"ENTER MACH NO & DIRECTION FOR CONTROL POINT 4";M4,D4
190 SQ = SQR(M4*M4 - 1):N4 = G2*ATN(SQ/G2) - ATN(SQ):NC = (N4 + D4 + NR
    - DF)/2:DC = (N4 + D4 - NF + DF)/2:NG = (NB + DB + N4 - D4)/2:DG =
    (NB + DB - N4 + D4)/2
195 W = PI/2 - 00*NC↑P - 01*NC↑.9:MC = 1/SIN(W):W = PI/2 - 00*NG↑P -
    01*NG .9:MG = 1/SIN(W)
200 PRINT"MC = ";MC, "DC = ";DC:PRINT"MG = ";MG, "DG = ";DG:PRINT"ENTER
    1 TO CONTINUE":PRINT" 2 TO REVISE CONTROL POINT 4":INPUT0:ONOGOTO
    220, 170
220 D5 = D4:M5 = 1 001:PRINT" CONTROL POINT 5 IS PRESET AT M5 = ";M5;"
    D5 = ";D5
225 INPUT"ENTER NEW ESTIMATES FOR M5 AND D5";M5,D5:SQ = SQR(M5*M5 - 1):
    N5 = G2*ATN(SQ/G2) - ATN(SQ):NX = (N5 + D5 + N4 - D4)/2:W = PI/2 -
    00*NX↑P - 01*NX↑.9:MX = 1/SIN(W):NY = (N4 + D4 + N5 - D5)/2:W = PI/2
    - 00*NY↑P - 01*NY↑.9:MY = 1/SIN(W)
230 PRINT"MX = ";MX,"MY = ";MY:PRINT"ENTER 1 TO ANALYZE NOZZLE IN FINE
    GRID ":PRINT" 2 TO REVISE ESTIMATE FOR M5 OR D5": PRINT" 3 TO
    RE-INITIATE THE COARSE GRID":INPUT0:ONOGOTO235, 225, 150

```

```

235 DX = (N5 + D5 - N4 + D4)/2: DY = (N4 + D4 - N5 + D5)/2
240 REM TRANSITION SEGMENT
245 IF O9 = 1 THEN 250 ELSE 1000
250 J4 = 1: J5 = 6: NO = (NB - NA)/8: N9 = (NF - NE)/8: GOSUB 260
255 J4 = 7: J5 = 10: NO = (NB - NU(6))/4: N9 = (NF - NL(6))/4: GOSUB 260
257 GOTO 292
260 FOR J = J4 TO J5
265 GOSUB 300
270 NU(J) = NU(J - 1) + NO: N = NU(J): WU(J) = PI/2 - 00*N↑P - 01*N↑.9:
    N(0) = NU(J): W(0) = WU(J): L(0) = L(11): D(0) = N(0) - L(0): DU(J) =
    D(0): R(0) = N(0) + D(0)
275 QW = TAN(DU(J)/2 + DU(J - 1)/2): QL = TAN((D(11) + W(11) + D(0) +
    W(0))/2): X(0) = (YU(J - 1) - Y(11) - QW*XU(J - 1) + QL*X(11))/(QL -
    QW): XU(J) = X(0): Y(0) = YU(J - 1) + QW*(XU(J) - XU(J - 1)): YU(J) = Y(0)
280 NL(J) = NL(J - 1) + N9: N = NL(J): WL(J) = PI/2 - 00*N↑P - 01*N↑.9:
    N(10) = NL(J): W(10) = WL(J): R(10) = R(20): D(10) = R(10) - N(10): DL(J)
    = D(10): L(10) = N(10) - D(10)
285 QW = TAN(DL(J)/2 + DL(J - 1)/2): QR = TAN((D(20) - W(20) + D(10) -
    W(20) + D(10) - W(10))/2): X(10) = (YL(J - 1) - Y(20) - QW*XL(J - 1)
    + QR*X(20))/(QR - QW): XL(J) = X(10): Y(10) = YL(J - 1) + QW*(XL(J) -
    XL(J - 1)): YL(J) = Y(10)
290 NEXT J: RETURN
292 PRINT "TRANSITION SEGMENT COMPLETED"
294 FOR I = 0 TO 20: X2(I) = X(I): Y2(I) = Y(I): D2(I) = D(I): N2(I) = N(I):
    W2(I) = W(I): R2(I) = R(I): L2(I) = L(I): NEXT I
295 GOTO 1000
300 FOR R = 0 TO 9: L = R + 1: K = R + 11: GOSUB 305: NEXTR: FOR R = 11 TO 19:
    L = R + 1: K = R - 10: GOSUB 305: NEXTR: RETURN
305 R(K) = R(R): L(K) = L(L): N(K) = R(K)/2 + L(K)/2: D(K) = R(K)/2 -
    L(K)/2: N = N(K): W(K) = PI/2 - 00*N↑P - 01*N↑.9
310 QR = TAN((D(R) - W(R) + D(K) - W(K))/2): QL = TAN((D(L) + W(L) +
    D(K) + W(K))/2): X(K) = (Y(L) - Y(R) + QR*X(R) - QL*X(L))/(QR - QL):
    Y(K) = Y(R) + QR*(X(K) - X(R))
315 RETURN

```

```

1000 REM INITIAL SETUP
1005 R5 = N5 + D5:L5 = N5 = D5
1010 FORJ = 30TO40
1015 NU(J) = NX + (J - 30)/10*(N5 - NX):NL(J) = NY + (J - 30)/10*(N5
    - NY):DU(J) = R5 - NU(J):DL(J) = NL(J) - L5:N = NU(J):WU(J) = PI/2
    - 00*N↑P - 01*N↑.9:N = NL(J):WL(J) = PI/2 - 00*N↑P - 01*N↑.9
1020 NEXTJ
1025 NB = NU(10):NF = NL(10)
1030 FOR J = 10TO20
1035 NU(J) = NB + (J - 10)/10*(NC - NB):NL(J) = NF + (J - 10)/10*(NC
    - NF):DU(J) = NU(J) - NL(J - 10) + DL(J - 10):DL(J) = NU(J - 10) +
    DU(J - 10) - NL(J):N = NU(J):WU(J) = PI/2 - 00*N↑P - 01*N↑.9
1040 N = NL(J):WL(J) = PI/2 - 00*N↑P - 01*N↑.9:NEXTJ
1045 FORJ = 21TO29
1050 NL(J) = (NU(J - 10) + DU(J - 10) + NU(J + 10) - DU(J + 10))/2:DL(J)
    = (NU(J - 10) + DU(J - 10) - NU(J + 10) + DU(J + 10))/2:N = NL(J):
    WL(J) = PI/2 - 00*N↑P - 01*N↑.9
1055 NU(J) = (NL(J + 10) + DL(J + 10) + NL(J - 10) - DL(J - 10))/2:DU(J)
    = (NL(J + 10) + DL(J + 10) - NL(J - 10) + DL(J - 10))/2:N = NU(J):
    WU(J) = PI/2 - 00*N↑P - 01*N↑.9:NEXTJ
1057 PRINT" SURFACE MACH NUMBER & FLOW ANGLE (DEG)":PRINT"STN";TAB(16)
    "UPPER";TAB(42)"LOWER":I1 = 10:12 = 0
1060 FORK = 0TO3:I1 = I1 = I1 + 10:I2 = I2 + 10:FORI = I1TO12:PRINTI;
    TAB(10)1/SIN(WU(I));TAB(22)DU(I)*57.3;TAB(37)1/SIN(WL(I));TAB(49)
    DL(I)*57.3:NEXTI:INPUT:NEXTK
1062 PRINT"ENTER 1 TO COMPLETE THE FINE GRID":PRINT" 2 TO REVISE
    THE COARSE NET":O9 = 2:INPUTO:ONOGOTO1065,165
1065 FORJ = 11TO35:GOSUB300:D(10) = DL(J):W(10) = WL(J):N(10) = NL(J):
    L(10) = N(10) - D(10)
1070 QW = TAN(DL(J - 1)/2 + DL(J)/2:QR = TAN(D(20) - W(20) + D(10) -
    W(10))/2):X(10) = (YL(J - 1) - Y(20) - QW*XL(J - 1) + QR*X(20))/
    (QR - QW):XL(J) = X(10):Y(10) = YL(J - 1) + QW*(XL(J) - XL(J - 1)):
    YL(J) = Y(10)

```

```

1075 D(0) = DU(J):W(0) = WU(J):N(0) = NU(J):R(0) = N(0) + D(0)
1080 QW = TAN(DU(J - 1)/2 + DU(J)/2):QL = TAN((D(11) + W(11) + D(0) +
      W(0))/2):X(0) = (YU(J - 1) - Y(11) - QW*XU(J - 1) + QL*X(11))/(QL -
      QW):XU(J) = X(0):Y(0) = YU(J - 1) + QW*(XU(J) - XU(J - 1)):YU(J) =
      Y(0)
1085 NEXTJ
1200 R = 10:L = 0
1210 FOR J = 30 TO 40
1220 R = R - 1:L = L + 1:DU(J) = D(L):WU(J) = W(L):DL(J) = D(R):WL(J) =
      W(R)
1230 QW = TAN(DU(J - 1)/2 + DL(J)/2):QL = TAN(D(L) + W(L)):XU(J) = (YU
      (J - 1) - Y(L) - QW*XU(J - 1) + QL*X(L))/(QL - QW):YU(J) = YU(J - 1)
      + QW*(XU(J) - XU(J - 1))
1235 QW = TAN(DL(J - 1)/2 + DL(J)/2):QR = TAN(D(R) - W(R)):XL(J) = (YL
      (J - 1) - Y(R) - QW*XL(J - 1) + QR*X(R))/(QR - QW):YL(J) = YL(J - 1)
      + QW*(XL(J) - XL(J - 1))
1240 NEXTJ
1250 GOTO5000
1300 LPRINT"TERMINAL MACH NO<1":GOTO5050
5000 REM BOUNDARY PRINTOUT
5010 LPRINTCHR$(29)" ":PRINT" ":LPRINT"UPPER NOZZLE BOUNDARY":LPRINT"
      ":LPRINT" X", "Y", "ANGLE", "MACH NO":LPRINT" "
5020 FOR J = 0 TO 40:LPRINTXU(J), YU(J), DU(J)*180/PI,1/SIN(WU(J)):NEXTJ
5030 LPRINT" ":LPRINT" ":LPRINT"LOWER NOZZLE BOUNDARY":LPRINT" ":LPRINT"X",
      "Y", "ANGLE", "MACH NO":LPRINT" "
5040 FORJ = 0 TO 40:LPRINTXL(J),YL(J),DL(J)*180/PI,1/SIN(WL(J)):NEXTJ
5050 LPRINT" ":LPRINT" ":LPRINTCHR$(30)" "
5060 LPRINT"CONTROL POINT INPUT":LPRINT" ":LPRINT"M2 = ";M2,"D2 = ";D2:
      LPRINT" ":LPRINT"M4 = ";M4,"D4 = ";D4:LPRINT"M5 = ";M5,"D5 = ";D5:
      LPRINT" ":LPRINTCHR$(29)" ":LPRINT" "
5100 CLS:PRINT"FOR REFERENCE: ":PRINT"MB = ";MB,"MC = ";MC,"MD = ";MD,
      "MX = ";MX:PRINT"MF = ";MF,"MG = ";MG,"MH = ";MH,"MY = ";MY:PRINT:
      PRINT" AND THE INPUT TO THE CONTROL POINTS WAS:":PRINT"M4 = ";M4,"M5
      = ";M5

```

```

5105 PRINT"D4 = ";D4,"D5 = ";D5:PRINT
5110 PRINT"FOR ANOTHER ATTEMPT - ENTER 1 TO RE-INITIATE A COARSE GRID"
      :PRINT,,"OR":PRINT"ENTER 2 TO PROCEED WITH BOUNDARY LAYER ANALYSIS"
      :INPUTO:ONOGOTO5115,5200
5115 PRINT"SETTING UP FOR COARSE GRID":O9 = 2:FORI = 0TO20:X(I) = X2(I):
      Y(I) = Y2(I):D(I) = D2(I):N(I) = N2(I):W(I) = W2(I):R(I) = R2(I):
      L(I) = L2(I):NEXTI:GOTO165
5200 CLS:PRINT"BOUNDARY LAYER ANALYSIS":PRINT" ENTER VALUES FOR THE FOL-
      LOWING PARAMETERS":PRINT" (DEFAULT VALUES ARE INDICATED)"
5210 YH = .5/12:XT = 3*YH:PT = PR*14.5:TT = 535
5220 PRINT"NOZZLE EXHAUST HEIGHT = ";YH;"FEET":INPUTYH:PRINT"ESTIMATED
      EFFECTIVE PRE-THROAT DISTANCE = ";XT;"FEET":INPUTXT:PRINT"STAGNATION
      PRESSURE = ";PT;"PSIA":INPUTPT:PRINT"STAGNATION TEMPERATURE = ";TT:
      "DEG R"
5225 PT = PT*144:INPUTTT:RM = SQR(1.4/1715)*(500 + 198.7)/2.27*100000000
      *PT/TT1.667
5230 REM REF TEMP (ABOVE) SET AT 500 R & PRETHROAT M (BELOW) AT .5
5235 MO = .5:RE = RM*MO/(1 + .2*MO*MO)12.333:TH = .036*XT/(RE*XT)1.2:
      D5 = (1.3 + .46*MO*MO)*TH:DS = DS*.6:TH = DS/1.76*PRINT"B L THICKNESS
      AT THROAT ARE:":PRINT,"DISPLACEMENT = ";DS;"FEET":PRINT,"MOMENTUM
      = ";TH;"FEET":INPUT
5240 CLS:PRINT"CALCULATION OF NOZZLE BOUNDARY LAYERS IS IN PROGRESS"
5250 TU = TH:TL = TH:SF = YH/10
5300 REM MAIN B L ROUTINE
5305 PRINT" DISPLACEMENT THICKNESS (INS)": PRINT"STN", "UPPER","LOWER"
5310 FOR J = 39TO0STEP-1
5320 MU = 1/SIN(WU(J)):ML = 1/SIN(WL(J)):MO = MU - 1/SIN(WU(J + 1)):
      M9 = ML - 1/SIN(WL(J + 1))
5330 TO = MO*TU*(3.3 - .54*MU*MU)/MU/(1 + .2*MU*MU):T9 = M9*TL*(3.3 -
      .54*ML*ML)/ML/(1 + .2*ML*ML)
5340 RU = RM*MU/((1 + 2*MU*MU)12.333)*TU:RL = RM*ML/((1 + 2*ML*ML)12.333
      *TL

```

```

5350 CO = ((LOG(RU))I1.838)*(RUI.05)*((1 + .144*MU*MU)I.578):CY = .1131/
      CO*(XU(J + 1) - XU(J))*SF:C9((LOG(RL))I1.838*(RLI.05)*((1 + .144*ML*
      ML)I.578:CL = .1131/C9*(XL(J + 1) - XL(J))*SF
5360 TU = TU + CU - TO:TL = TL + CL - T9
5370 SU(J) = TU*(1.3 + .46*MU*MU):SL(J) = TL*(1.3 + .46*ML*ML)
5380 YT(J) = YU(J)*SF + SU(J):YB(J) = YL(J)*SF - SL(J)
5385 PRINTJ,SU(J)*12,SL(J)*12
5390 NEXT J
5400 REM NOZZLE COORDS PRINTOUT
5410 LPRINTCHR$(30)" ":LPRINT"NOZZLE CONTOURS (INCHES)":LPRINT"":LPRINT"
      UPPER SURFACE":LPRINT" ":LPRINT" X"," Y":LPRINT" ":FORI = 0TO38:
      LPRINTXU(I)*SF*12,YT(I)*12 + SL(0)*12:NEXTI
5415 FF = 1:HX = XU(38):KY = (YT(38) + SL(0))/SF:FORXX = 0TO18STEP.5:
      GOSUB5500:NEXTXX:LPRINT" "
5420 LPRINT" ":LPRINT"LOWER SURFACE":LPRINT" ":LPRINT" X"," Y":LPRINT"
      ":FORI = 0TO39:LPRINTXL(I)*SF*12,YB(I)*12 + SL(0)*12:NEXTI
5425 FF = - 1:HX = XL(39):KY = (YB(39) + SL(0))/SF:FORXX = 0TO18STEP.5:
      GOSUB5500:NEXTXX:LPRINT"":LPRINTCHR$(29)" "
5450 PRINT"NOZZLE ANALYSIS PROGRAM END":STOP
5500 REM SUB FOR SUBSONIC INLET
5510 YY = (XXI3/1008.2 - XXI4/297030.)*FF
5520 XU = XX*COS(D5) - YY*SIN(D5) + HX:YU = XX*SIN(D5) + YY*COS(D5) + KY
5530 LPRINTXU*SF*12,YU*SF*12
5540 RETURN

```

APPENDIX B

Vortex Profile Nozzle

X	Upper Surface	Lower Surface
0	.540	0
.10	.538	-.001
.20	.532	-.005
.30	.523	-.012
.40	.509	-.022
.50	.492	-.035
.60	.471	-.052
.70	.448	-.070
.80	.422	-.091
.90	.395	-.115
1.00	.365	-.139
1.05	.351	-.151 (throat)
1.10	.333	
1.21	.307 (throat)	

Convergent-Divergent Nozzle

X	Upper Surface	Lower Surface
0	.507	0
.10	.506	.001
.20	.505	.002
.30	.503	.004
.40	.502	.005
.50	.500	.007
.60	.499	.008
.70	.498	.009
.80	.497	.010
.90	.496 (throat)	.011 (throat)

REFERENCES

1. Metral, A., Zerner, F., "The Coanda Effect," Publication Scientifiques et Techniques du Ministere de l'Air, No. 218 (1948); M.O.S., TIB/T4027 (1953).
2. Davenport, F. J., Hunt, D. N., "Deflection of a Thick Jet by a Convex Surface: A Practical Problem for Powered Lift," AIAA Paper 75-167, AIAA 13th Aerospace Sciences Meeting, Pasadena, California, Jan. 20-22, 1975.
3. Covault, C., "Upper-Surface Blowing Cost Gains Cited," Aviation Week & Space Technology, 13 May 1974, p. 55.
4. Throndson, L. W., "Compound Ejector Thrust Augmenter Development," ASME Paper No. 73-GT-67, Gas Turbine Conference and Products Show, Washington, D.C., April 8-12, 1973.
5. Englar, R. J., "Test Techniques for High Lift Two-Dimensional Airfoils with Boundary Layer and Circulation Control Application to Rotary Wing Aircraft," Canadian Aeronautics and Space Journal, Vol. 19, No. 3, March 1973, pp. 93-105.
6. Whitten, P. D., Kennon, I. G., and Stumpfl, S. C., "Experimental Investigation of a Nozzle/Wing Propulsive Lift Concept," AIAA Paper No. 76-265, AIAA/SAE 12th Propulsion Conference, Palo Alto, Calif., July 26-29, 1976.
7. Child, R. D., Henderson, W. P., "Canard Configured Aircraft with 2-D Nozzle," Rockwell International Report NA-78-311, August 1978.
8. Guile, R. N., Hilding, W. E., "Investigation of a Free-Vortex Aerodynamic Window," AIAA Paper 75-122, AIAA 13th Aerospace Sciences Meeting, Pasadena, California, January 20-22, 1975.
9. Bradbury, L. J. S., Wood, M. N., "An Exploratory Investigation into the Deflection of Thick Jets by the Coanda Effect," Royal Aircraft Establishment, Technical Report No. 65235, October 1965.
10. Von Glahn, U., and Groesbeck, D., "Effect of External Jet-Flow Deflector Geometry on Over-the-Wing Aero-Acoustic Characteristics," NASA TM X-73460, 1976.
11. Newman, B. G., "Deflection of Plane Jets by Adjacent Boundaries - Coanda Effect," Article in Boundary Layer and Flow Control, Its Principles and Application, Pergamon Press, 1961.

12. Von Glahn, U., "Use of the Coanda Effect for Jet Deflection and Vertical Lift with a Multiple-Flat-Plate and Curved-Plate Deflection Surfaces," NACA TN 4377, September 1958.
13. Liepman, H. W. and Roshko, A., "Elements of Gas Dynamics," J. Willet and Sons.
14. Dayman, B., "Comparison of Calculated with Measured Boundary Layer Thicknesses on the Curved Walls of the JPL 20-inch Supersonic Wind Tunnel Two-Dimensional Nozzle," JPL-TR No. 32-349, 1963.
15. Guitton, D. E., Newman, B. G., "Self-Preserving Turbulent Wall Jets Over Convex Surfaces," J. Fluid Mech. (1977), Vol. 81, Part I, pp. 155-185.